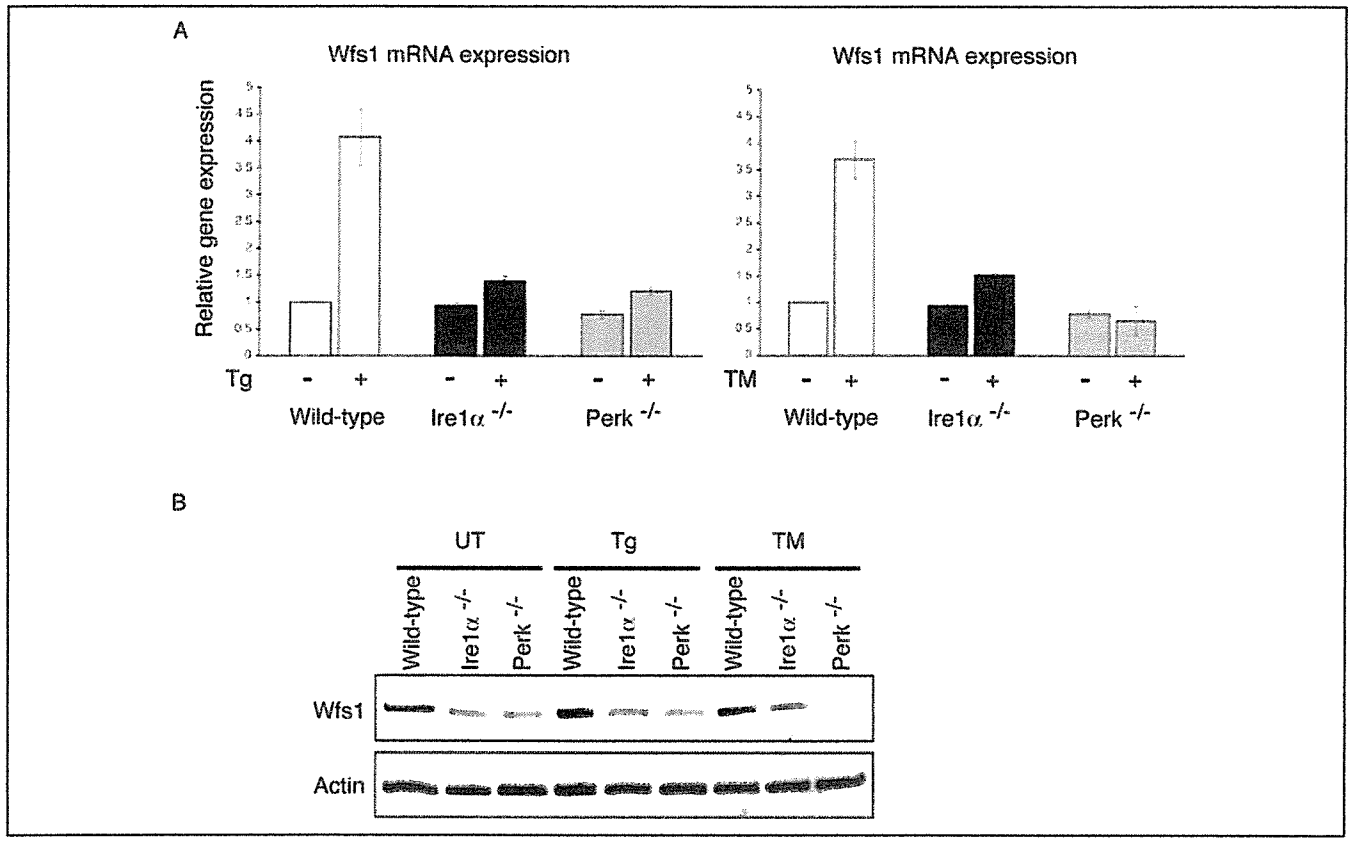

FIGURE 1. **Expression of WFS1, a component of the UPR, is regulated by Ire1α.** *A*, quantitative real time PCR of WFS1 using reverse-transcribed RNA from wild-type, Ire1α knock-out (Ire1$\alpha^{-/-}$), and Perk knock-out (Perk$^{-/-}$) mouse embryonic fibroblasts. Cells were untreated (*UT*) or treated with thapsigargin (*Tg*) or tunicamycin (*TM*) for 3 h. The amount of mouse WFS1 mRNA was normalized to the amount of actin mRNA in each sample (n = 3; values are mean ± S.E.). *B*, immunoblot analysis of WFS1 protein using lysates from wild-type, Ire1α knock-out (Ire1$\alpha^{-/-}$), and Perk knock-out (Perk$^{-/-}$) mouse embryonic fibroblasts. Cells were untreated or treated with thapsigargin (*Tg*) or tunicamycin (*TM*) for 3 h. The amount of actin is shown in the *lower panel*.

in the *EIF2AK3* gene encoding PERK have been reported (32). PERK knock-out mice also develop diabetes because of the high level of ER stress in the pancreas (33, 34), strongly suggesting that β-cell death in patients with Wolcott-Rallison syndrome is caused by ER stress. ATF6 is a bZIP-containing transcription factor in the ER. Under ER stress, ATF6 is cleaved and released from the ER. The bZIP domain of ATF6 then translocates into the nucleus and up-regulates the UPR-specific downstream genes. The physiological role of ATF6 in pancreatic β-cells is not yet known.

Increasing evidence suggests that a high level of ER stress and defective ER stress signaling are important in the pathogenesis of diabetes. It is highly likely that downstream components of ER stress signaling maintain ER homeostasis in pancreatic β-cells. Therefore, defective ER stress signaling could cause a high level of ER stress in pancreatic β-cells and lead to β-cell dysfunction and diabetes. Pancreatic β-cells are specialized in proinsulin folding and insulin secretion. It is possible that β-cells have a unique downstream component of ER stress signaling. In this study we investigated whether Wolfram syndrome gene 1 (*WFS1*) is a component of ER stress signaling and has a function in maintaining ER homeostasis in β-cells.

EXPERIMENTAL PROCEDURES

Plasmids, Cell Culture, and Transfection—INS-1 832/13 cells were a gift from Dr. Christopher Newgard (Duke University Medical Center). INS-1 832/13 cells were maintained in RPMI with 10% fetal bovine serum and transfected with siRNA for WFS1 using the Cell Line Nucleofector™ T kit and the Nucleofector device (Amaxa Biosystems, Gaithersburg, MD). siRNAs were designed and synthesized at Qiagen (Valencia, CA) as follows: for rat WFS1–1, AAGGCATGAAGGTCTACAATT; for rat WFS1–2, AAGGCCATCAGCTGCCTCAAT. COS7 cells were maintained in Dulbecco's modified Eagle's medium with 10% fetal bovine serum and then transfected with WFS1 expression vectors using FuGENE (Roche Applied Science). Full-length human *WFS1* cDNA, as well as P724L and G695V mutant *WFS1* cDNA, were tagged with a FLAG epitope and subcloned to a pcDNA3 plasmid under the control of the cytomegalovirus promoter. The P724L and G695V mutations were introduced using the GeneTailor site-directed mutagenesis system (Invitrogen). Mouse embryonic fibroblasts were maintained in Dulbecco's modified Eagle's medium with 10% fetal bovine serum. Human fibroblasts of a patient with Wolfram syndrome and a control individual were obtained, respectively, from Coriell Institute (Camden, NJ) and from Dr. Alan Permutt (Washington University School of Medicine). Human fibroblasts were maintained in Eagle's modified essential medium with 10% fetal bovine serum.

Immunostaining—COS7 cells and frozen sections of mouse pancreata were fixed in 2% paraformaldehyde for 30 min at room temperature and then permeabilized with 0.1% Triton X-100 for 2 min. The fixed cells were washed with phosphate-buffered saline, blocked with 10% bovine serum albumin for 30 min, and incubated in primary antibody overnight at 4 °C. The cells were washed three times in phosphate-buffered saline/Tween 0.1% and incubated with secondary antibody for 1 h at room temperature. Images were obtained with a Leica TCS SP2 AOBS confocal microscope with LCS software. FLAG M2 antibody was

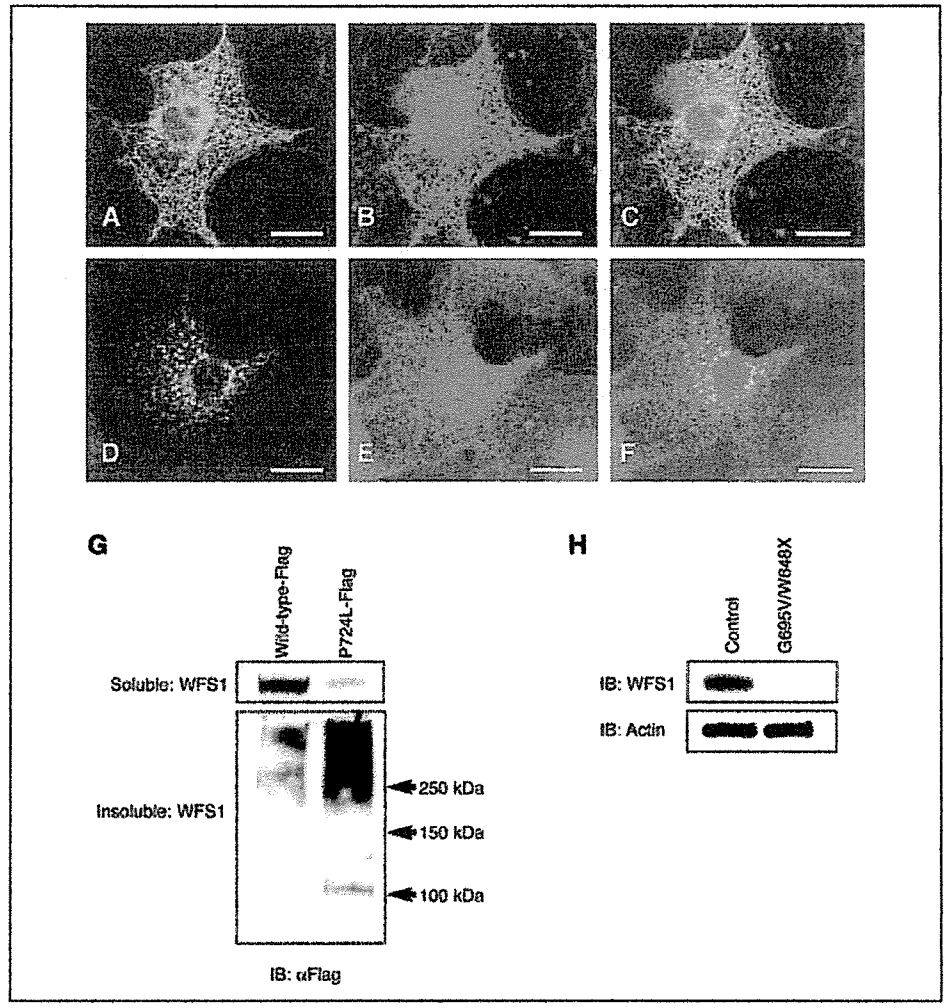

FIGURE 2. **Loss of function of WFS1 on ER membrane causes Wolfram syndrome.** Immunocytochemical staining of COS7 cells expressing FLAG-tagged human wild-type (*A–C*) or P724L WFS1 (*D–F*). Staining with anti-FLAG monoclonal antibody shows the distribution of wild-type or P724L WFS1 protein (*A* and *D*). Staining of the same cells with anti-ribophorin I antibody shows the structure of the ER (*B* and *E*). Merged images show the co-localization of WFS1 and ribophorin I (*C* and *F*). *Bars*, 10 μm. *G*, high molecular weight complexes of $WFS1^{P724L}$ in detergent-insoluble fractions. COS7 cells were transfected with FLAG-tagged wild-type or P724L WFS1 expression vector and separated into detergent-soluble (*upper panel*) and detergent-insoluble (*lower panel*) fractions and immunoblotted (*IB*) with anti-FLAG antibody. *H*, immunoblot analysis of WFS1 protein using lysates from fibroblasts of a control individual (*control*) and a patient with Wolfram syndrome carrying G695V/W648*X* mutations (G695V/W648X).

purchased from Sigma. Anti-WFS1 antibody was generated as described previously (35).

Immunoblotting—Fibroblasts and INS-1 832/13 cells were lysed with M-PER (Pierce) containing protease inhibitors. COS7 cells were lysed for 15 min in ice-cold buffer (20 mM Hepes, pH 7.5, 1% Triton X-100, 150 mM NaCl, 10% glycerol, 1 mM EDTA) containing protease inhibitors. Insoluble material was recovered by centrifugation at 13,000 × *g* for 15 min and solubilized in 10 mM Tris-HCl and 1% SDS for 10 min at room temperature. After the addition of 4 volumes of lysis buffer, samples were sonicated for 10 s. Lysates were separated and normalized for total protein (20 μg per lane) using 4–20% linear gradient SDS-PAGE (Bio-Rad) and then electroblotted. FLAG M2 antibody was purchased from Sigma. Anti-WFS1 antibody was generated as described previously (35).

Isolating Islets from Mouse Pancreas—Mice were anesthetized, and their pancreatic islets were then isolated by pancreatic duct injection of 5 ml (0.85 mg/ml) of collagenase solution followed by digestion at 37 °C for 25 min with mild shaking. Digestion was stopped by adding ice-cold RPMI with 1% horse serum. Islets were washed several times with RPMI, separated from acinar cells on a Histopaque gradient, and hand-picked using a dissecting microscope.

Real Time PCR—Total RNA was isolated from the cells by RNeasy (Qiagen, Valencia, CA). 1 μg of total RNA from cells was reverse-transcribed with oligo(dT) primer. For the thermal cycle reaction, the ABI prism 7000 sequencer detection system (Applied Biosystems, Foster City, CA) was used at 50 °C for 2 min, 95 °C for 10 min, then 40 cycles at 95 °C of 15 s each, and at 60 °C for 1 min. By using mouse actin for mouse embryonic fibroblasts, human glyceraldehyde-3-phosphate dehydrogenase for human fibroblasts, mouse actin for mouse islets, and rat actin for INS-1 832/13 cells as a control, the PCR was performed in triplicate for each sample and then repeated twice for all experiments. Cyber Green (Bio-Rad) and the following sets of primers were used for real time PCR: for mouse actin, GCAAGTGCTTCTAGGCGGAC and AAGAAAGGGTGTAAAACGCAGC; for mouse WFS1, CCATCAACATGCTCCCGTTC and GGGTAGGCCTCGCCATACA; for rat actin, GCAAATGCTTCTAGGCGGAC and AAGAAAGGGTGTAAAACGCAGC; and for rat WFS1, CATCACCAAGGACATCGTCCT and AGCACGTCCTTGAACTCGCT.

RESULTS

WFS1 Is a Component of the IRE1 Signaling Pathway—The pathogenesis of Wolfram syndrome has been attributed to mutations in the *WFS1* gene (35, 36). The *WFS1* gene encodes a 100-kDa glycoprotein containing 9–10 transmembrane domains that localizes to the ER (5, 6). Membrane proteins in the ER are often involved in the UPR (8, 37).

Measuring the expression levels of WFS1 by real time PCR, we found that WFS1 mRNA is induced by ER stress and is under the control of IRE1α and PERK. In wild-type mouse fibroblasts, induction of WFS1 mRNA was increased 3–5-fold by two ER stress inducers, tunicamycin and thapsigargin (Fig. 1*A*).

In Ire1$\alpha^{-/-}$ and Perk$^{-/-}$ cells, WFS1 induction was attenuated (Fig. 1*A*). By measuring WFS1 protein expression levels by immunoblot using anti-WFS1 antibody, we found that WFS1 protein expression was decreased in Ire1$\alpha^{-/-}$ and Perk$^{-/-}$ cells as compared with wild-type cells (Fig. 1*B*). Although there was a marked induction of WFS1 mRNA in wild-type cells by both inducers of ER stress (Fig. 1*A*), induction of WFS1 at the protein level in tunicamycin-treated cells in which *N*-glycosylation was inhibited was modest (Fig. 1*B*), suggesting that the WFS1 protein is unstable when *N*-glycosylation is inhibited. Also, there was no significant difference in WFS1 mRNA content between wild-type cells and both knock-out cells, although at the protein level, both Ire1$\alpha^{-/-}$ and Perk$^{-/-}$ cells exhibited a profound decrease in WFS1 protein expression. This suggests further that WFS1 protein becomes unstable by chronic high levels of ER stress because there exists a higher base-line ER stress level in Ire1$\alpha^{-/-}$ and Perk$^{-/-}$ cells, which are deficient in ER stress signaling. These results indicate that WFS1 is a component of the UPR and that its mRNA expression is regulated by the IRE1 and PERK signaling pathways.

Mutant WFS1 Does Not Accumulate on the ER Membrane—It has been reported that *WFS1* gene mutations lead to loss of function of WFS1 protein. Nonsense or frameshift mutations of the *WFS1* gene lead to a complete absence of WFS1 protein because of instability of the mutant protein (36). To extend this observation, we examined the cellular localization of mutant WFS1 protein. Most of the *WFS1* gene mutations in patients with Wolfram syndrome occur in exon 8, which encodes the transmembrane of the protein and in C-terminal luminal domains (5, 6). We cloned the full-length human *WFS1* gene by using human EST clones and then introduced into it the P724L and G695V mutations, which occur in Wolfram syndrome, by means of PCR-based mutagenesis. Like most *WFS1* mutations in Wolfram syndrome patients, the P724L and G695V mutations occurred in exon 8.

We then determined the cellular localization of wild-type and mutant WFS1 by immunostaining cells transfected with an expression vector for wild-type, P724L, or G695V WFS1 tagged at its C terminus with a FLAG epitope. Immunostaining of cells expressing wild-type WFS1 showed a diffuse reticular pattern that co-localized with the ER marker ribophorin I (Fig. 2, *A–C*). However, immunostaining with anti-FLAG antibody of cells expressing mutant WFS1 showed a punctate staining pattern in the ER, suggesting that WFS1 tends to aggregate there (Fig. 2, *D–F*). Part of WFS1^{P724L} showed a diffuse reticular pattern and was co-localized with ribophorin I, suggesting that this part of WFS1^{P724L} is localized to the ER membrane (Fig. 2, *D–F*). These staining patterns suggest that, in contrast to wild-type WFS1, most of the newly synthesized WFS1^{P724L} protein aggregates and thus is not expressed on the ER membrane. We obtained similar results by expressing WFS1^{G695V} (data not shown).

When we assessed the aggregation of WFS1^{P724L} by SDS-PAGE immunoblot analysis of detergent-soluble and detergent-insoluble lysates from COS7 cells transiently expressing these proteins, we found that the formation of insoluble and high molecular weight complexes was much more prominent in cells expressing WFS1^{P724L} than in cells expressing wild-type WFS1 (Fig. 2*G*, *lower panel*).

We also measured WFS1 protein expression levels in fibroblasts from a patient with Wolfram syndrome and a control individual. We found that WFS1 protein could not be detected in the patient sample (Fig. 2*H*), suggesting that mutant WFS1 protein in patients with Wolfram syndrome does not accumulate in cells or can no longer be detected by the antibody because of a conformational change. Our results indicate that most of the newly synthesized mutant WFS1 protein tends to aggregate and does not fold into a proper three-dimensional structure. Therefore, it is likely that Wolfram syndrome is caused by a loss of function of WFS1.

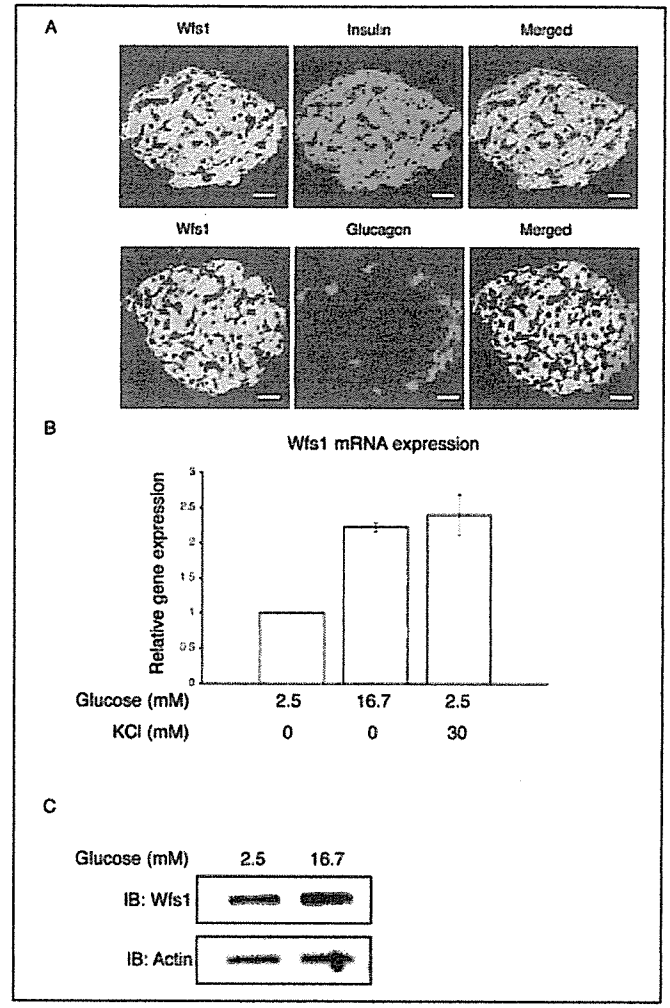

FIGURE 3. **WFS1 maintains ER homeostasis in pancreatic β-cells.** *A*, distribution of WFS1 in mouse pancreata analyzed by immunohistochemistry using anti-WFS1, anti-insulin, and anti-glucagon antibodies. Merged image shows the co-localization of WFS1 and insulin (*upper panel*) or WFS1 and glucagon (*lower panel*). *Scale bars*, 50 μm. *B*, WFS1 mRNA is up-regulated by insulin secretagogues. Mouse islets were pretreated with 2.5 mM glucose for 1 h and stimulated with 16.7 mM glucose and 30 mM KCl for 1 h. Expression levels of WFS1 and actin were then measured by real time PCR ($n = 3$; values are mean ± S.E.). *C*, WFS1 protein is up-regulated by high glucose. Mouse islets were pretreated with 2.5 mM glucose for 2 h and stimulated with 16.7 mM glucose. The expression levels of WFS1 and actin were measured by immunoblot (*IB*).

WFS1 Is Important in Sustaining ER Homeostasis in Pancreatic β-Cells—In immunohistochemistry experiments on mouse pancreata using anti-WFS1, anti-insulin, and anti-glucagon antibodies, we detected WFS1 mainly in the islets, where it co-localized with insulin (Fig. 3*A*). However, WFS1 did not co-localize with glucagon, indicating that WFS1 is especially important in the function of β-cells.

It has been shown that WFS1 has an important function in stimulus-secretion coupling in insulin secretion (38). To determine *WFS1* gene expression levels during insulin secretion, we pretreated mouse islets for 1 h with 2.5 mM glucose and then stimulated these cells for insulin secretion with 16.7 mM glucose and 30 mM KCl. *WFS1* gene expression increased after treatment with both 16.7 mM glucose and 30 mM KCl but not after treatment with 2.5 mM glucose (Fig. 3*B*), suggesting that WFS1 up-regulation is important for insulin secretion. By measuring WFS1

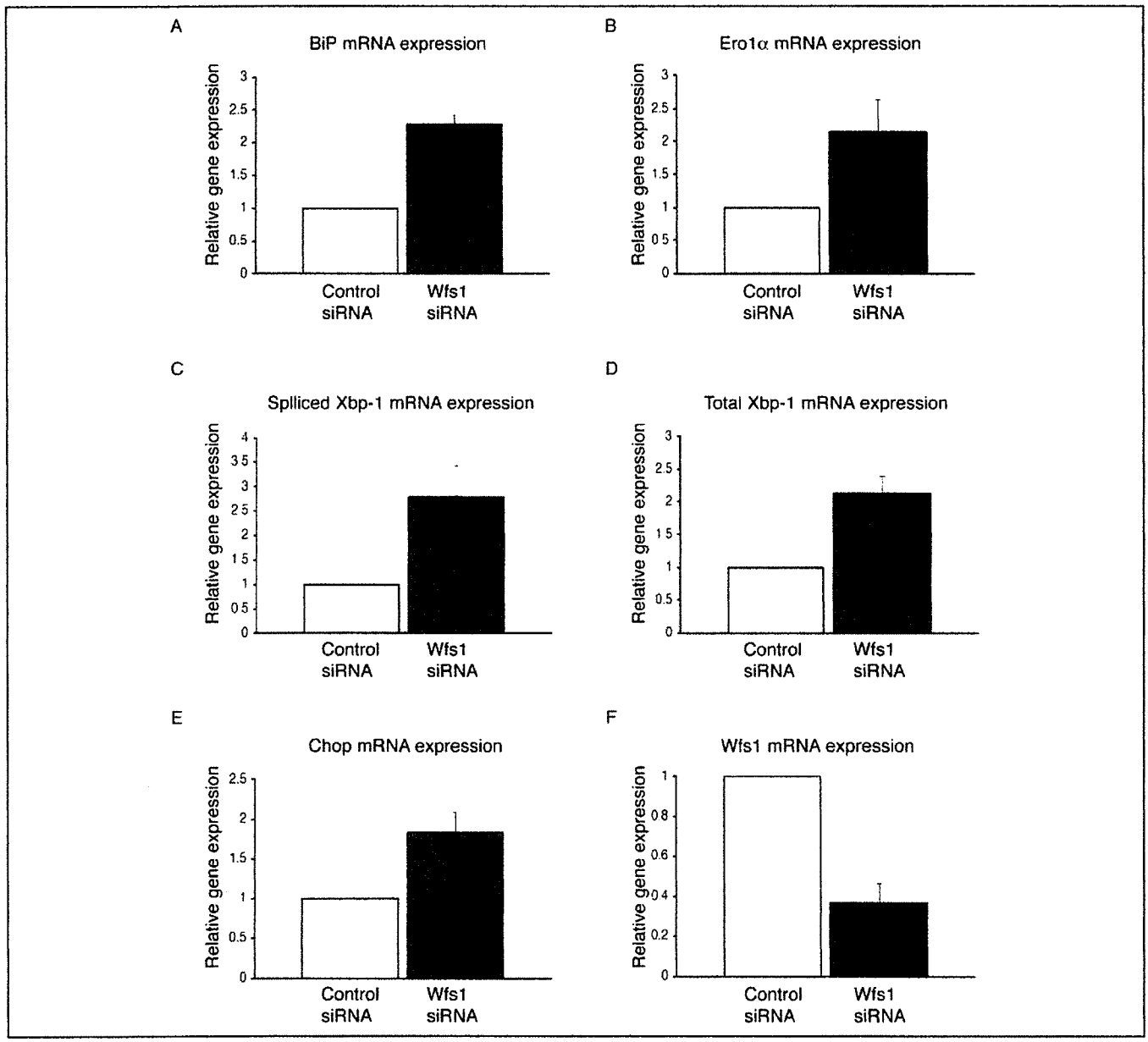

FIGURE 4. **Inhibition of WFS1 expression causes a high level of ER stress in pancreatic β-cells.** INS-1 832/13 cells were pretreated with 5 mM glucose and transfected with siRNA for WFS1 or scramble siRNA. Expression levels of the ER stress markers BiP (*A*), ERO1α (*B*), spliced XBP-1 (*C*), total XBP-1 (*D*), Chop (*E*), and WFS1 (*F*) were measured by real time PCR (n = 3; values are mean ± S.E.).

protein expression levels by immunoblot using anti-WFS1 antibody, we confirmed this WFS1 induction by 16.7 mM glucose in mouse islets (Fig. 3*C*).

ER homeostasis is important for insulin secretion because proinsulin, the insulin precursor, must be folded into its proper three-dimensional structure in the ER in order to become mature insulin. As a direct means of examining the relationship between the loss of function of WFS1 and ER homeostasis, we knocked down WFS1 expression in a β-cell line, INS-1 832/13, using siRNA for WFS1. The suppression of WFS1 caused an increase in the expression of BiP (Fig. 4*A*), Ero1α (Fig. 4*B*), spliced XBP-1 (Fig. 4*C*), and total XBP-1 (Fig. 4*D*), markers for ER stress in INS-1 832/13 cells. This suppression also increased the expression of another ER stress marker, Chop (Fig. 4*E*). However, the induction of Chop mRNA was modest as compared with its usual up-regulation under ER stress. Because Chop is a downstream component of Perk signaling (39), this suggests that eIF2α phosphorylation by Perk in response to WFS1 suppression is modest. Indeed, we could not detect eIF2α phosphorylation by suppressing WFS1 expression in INS-1 832/13 cells (data not shown). These results indicate that WFS1 has an important function in mitigating high levels of ER stress and in maintaining ER homeostasis in pancreatic β-cells. Therefore, suppression of WFS1 in β-cells could cause chronic ER stress in these cells.

To analyze the WFS1 expression level under pathological conditions, we measured WFS1 mRNA induction in islets from the ob/ob diabetes mouse model. We isolated islets from diabetic ob/ob mice and control C57Bl6 mice and measured WFS1 mRNA induction by treating the cells with 16.7 mM glucose. We found that induction of WFS1 mRNA was significantly more attenuated in ob/ob mice than in control mice (Fig. 5). This suggests that β-cells in ob/ob mice are in a state of chronic ER stress and that WFS1 induction is saturated.

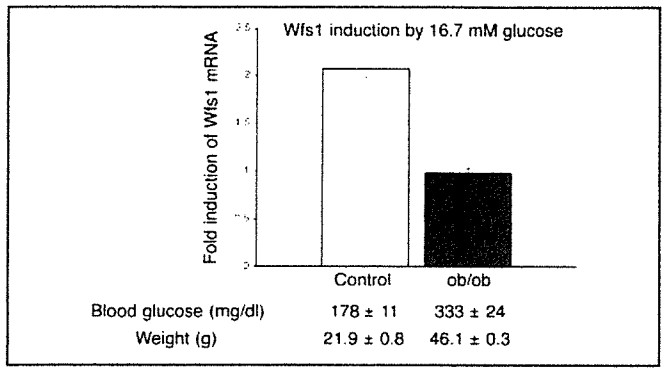

FIGURE 5. **WFS1 induction is attenuated in the islets of ob/ob mice.** Islets from control C57BL6 mice and ob/ob mice were isolated and pretreated with 2.5 mM glucose for 1 h and then stimulated with 2.5 or 16.7 mM glucose for 1 h. The expression levels of WFS1 and actin were measured by real time PCR, and the induction of WFS1 by 16.7 mM glucose was calculated ($n = 3$; values are mean ± S.E.)

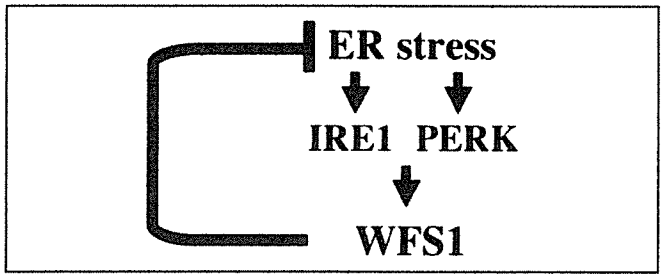

FIGURE 6. **Schematic model of the role of WFS1 in mitigating ER stress.** WFS1 is a component of IRE1 and PERK signaling (*i.e.* the UPR) and is important in the maintenance of ER homeostasis, specifically in pancreatic β-cells.

DISCUSSION

Our study has shown that WFS1 is a component of IRE1 and PERK signaling (*i.e.* the UPR) and is important in the maintenance of ER homeostasis, specifically in pancreatic β-cells (Fig. 6). *WFS1* mutations in patients with Wolfram syndrome lead to loss of function of WFS1. In addition, by using siRNA, we have shown that the suppression of WFS1 leads to a high level of ER stress in pancreatic β-cells. These findings suggest that WFS1 protects β-cells against ER stress and, conversely, that chronic ER stress is caused by loss of function of WFS1. Previous studies have shown that WFS1 protein serves as a regulator of the ER ion channel, most likely acting as a calcium channel (7, 36). It has also been reported that the increase in production of cytosolic Ca^{2+} in response to glucose is lower in the islets of WFS1 knock-out mice than it is in control mice (38). These findings suggest that loss of function of WFS1 causes abnormal calcium homeostasis in the ER and elicits ER stress, leading to the death of pancreatic β-cells.

Our findings suggest that the pathogenesis of Wolfram syndrome can be attributed to a very high level of chronic ER stress because of the lack of functional WFS1 protein in pancreatic β-cells (Fig. 4, *A–F*). WFS1 protein is expressed mainly in β-cells of the islets, but not in α-cells or exocrine acinar cells. Although α-cells and acinar cells are also active in protein secretion, WFS1 expression levels in these cells are much lower than those in β-cells that are specialized in insulin biosynthesis and secretion. Therefore, our findings of WFS1 expression only in β-cells and of WFS1 up-regulation during insulin secretion suggest that WFS1 is an important component of proinsulin folding and processing in the ER of β-cells.

Our results also show that pathogenic WFS1 mutants do not accumulate in the soluble fraction of cells and make insoluble aggregates. It is possible that the accumulation of pathogenic WFS1 mutants is toxic to pancreatic β-cells, causing them to malfunction in patients with Wolfram syndrome. Indeed, we found that transient expression of pathogenic WFS1 mutants caused ER stress in a pancreatic β-cell line, MIN6 (data not shown). However, stable expression of pathogenic WFS1 in MIN6 cells did not cause ER stress and did not change the viability of these cells.[4] These observations suggest that the expression of mutant WFS1 causes ER stress in pancreatic β-cells under specific conditions. It is also possible that ER stress response caused by transient and incomplete suppression of WFS1 with siRNA might differ from that caused by chronic and complete WFS1 deficiency. We plan to undertake additional studies to explore these possibilities.

The high levels of ER stress and pancreatic β-cell death in patients with Wolfram syndrome may be related to the β-cell dysfunction in patients with type 2 diabetes. The pathogenesis of type 2 diabetes is a result of peripheral resistance to the action of insulin, which may lead to a prolonged increase in insulin biosynthesis. Because the folding capacity of the ER is then overwhelmed, this peripheral resistance to insulin may activate the ER stress signaling pathways. For this reason, chronic ER stress in β-cells may lead to β-cell death in patients with type 2 diabetes who are genetically susceptible to ER stress. Further investigations of ER stress in the pathogenesis of diabetes are needed to obtain an understanding of the relationship between ER stress and type 2 as well as type 1B diabetes.

Acknowledgments—We thank Dr. Aldo Rossini, Dr. Rita Bortell, Dr. Shinsuke Ishigaki, Jeanne Cole, and Dr. Tomohiko Urano for comments on the manuscript. We thank Dr. Christopher Newgard for INS-1 832/13 and Dr. Alan Permutt for fibroblasts from a patient with Wolfram syndrome. We also thank Karen Sargent, Elaine Norowski, and Linda Leehy for technical assistance.

REFERENCES

1. Wolfram, D. J., and Wagener, H. P. (1938) *Mayo Clin. Proc.* **1,** 715–718
2. Barrett, T. G., and Bundey, S. E. (1997) *J. Med. Genet.* **34,** 838–841
3. Rando, T. A., Horton, J. C., and Layzer, R. B. (1992) *Neurology* **42,** 1220–1224
4. Karasik, A., O'Hara, C., Srikanta, S., Swift, M., Soeldner, J. S., Kahn, C. R., and Herskowitz, R. D. (1989) *Diabetes Care* **12,** 135–138
5. Inoue, H., Tanizawa, Y., Wasson, J., Behn, P., Kalidas, K., Bernal-Mizrachi, E., Mueckler, M., Marshall, H., Donis-Keller, H., Crock, P., Rogers, D., Mikuni, M., Kumashiro, H., Higashi, K., Sobue, G., Oka, Y., and Permutt, M. A. (1998) *Nat. Genet.* **20,** 143–148
6. Strom, T. M., Hortnagel, K., Hofmann, S., Gekeler, F., Scharfe, C., Rabl, W., Gerbitz, K. D., and Meitinger, T. (1998) *Hum. Mol. Genet.* **7,** 2021–2028
7. Osman, A. A., Saito, M., Makepeace, C., Permutt, M. A., Schlesinger, P., and Mueckler, M. (2003) *J. Biol. Chem.* **278,** 52755–52762
8. Harding, H. P., Calfon, M., Urano, F., Novoa, I., and Ron, D. (2002) *Annu. Rev. Cell Dev. Biol.* **18,** 575–599
9. Kaufman, R. J., Scheuner, D., Schroder, M., Shen, X., Lee, K., Liu, C. Y., and Arnold, S. M. (2002) *Nat. Rev. Mol. Cell. Biol.* **3,** 411–421
10. Mori, K. (2000) *Cell* **101,** 451–454
11. Harding, H. P., and Ron, D. (2002) *Diabetes* **51,** Suppl. 3, 455–461
12. Scheuner, D., Gromeier, M., Davies, M. V., Dorner, A. J., Song, B., Patel, R. V., Wimmer, E. J., McLendon, R. E., and Kaufman, R. J. (2003) *Virology* **317,** 263–274
13. Kaufman, R. J. (2002) *J. Clin. Investig.* **110,** 1389–1398
14. Tirasophon, W., Welihinda, A. A., and Kaufman, R. J. (1998) *Genes Dev.* **12,** 1812–1824
15. Iwawaki, T., Akai, R., Kohno, K., and Miura, M. (2004) *Nat. Med.* **10,** 98–102
16. Wang, X. Z., Harding, H. P., Zhang, Y., Jolicoeur, E. M., Kuroda, M., and Ron, D. (1998) *EMBO J.* **17,** 5708–5717
17. Bertolotti, A., Wang, X., Novoa, I., Jungreis, R., Schlessinger, K., Cho, J. H., West, A. B., and Ron, D. (2001) *J. Clin. Investig.* **107,** 585–593
18. Calfon, M., Zeng, H., Urano, F., Till, J. H., Hubbard, S. R., Harding, H. P., Clark, S. G., and Ron, D. (2002) *Nature* **415,** 92–96
19. Yoshida, H., Matsui, T., Hosokawa, N., Kaufman, R. J., Nagata, K., and Mori, K. (2003) *Dev. Cell* **4,** 265–271
20. Urano, F., Wang, X., Bertolotti, A., Zhang, Y., Chung, P., Harding, H. P., and Ron, D.

[4] S. G. Fonseca, M. Fukuma, K. L. Lipson, L. X. Nguyen, J. R. Allen, Y. Oka, and F. Urano, unpublished observations.

(2000) *Science* **287,** 664–666
21. Hoeflich, K. P., Yeh, W. C., Yao, Z., Mak, T. W., and Woodgett, J. R. (1999) *Oncogene* **18,** 5814–5820
22. Nishitoh, H., Saitoh, M., Mochida, Y., Takeda, K., Nakano, H., Rothe, M., Miyazono, K., and Ichijo, H. (1998) *Mol. Cell* **2,** 389–395
23. Nishitoh, H., Matsuzawa, A., Tobiume, K., Saegusa, K., Takeda, K., Inoue, K., Hori, S., Kakizuka, A., and Ichijo, H. (2002) *Genes Dev.* **16,** 1345–1355
24. Ozcan, U., Cao, Q., Yilmaz, E., Lee, A. H., Iwakoshi, N. N., Ozdelen, E., Tuncman, G., Gorgun, C., Glimcher, L. H., and Hotamisligil, G. S. (2004) *Science* **306,** 457–461
25. Yoneda, T., Imaizumi, K., Oono, K., Yui, D., Gomi, F., Katayama, T., and Tohyama, M. (2001) *J. Biol. Chem.* **276,** 13935–13940
26. Nakagawa, T., Zhu, H., Morishima, N., Li, E., Xu, J., Yankner, B. A., and Yuan, J. (2000) *Nature* **403,** 98–103
27. Yoshida, H., Haze, K., Yanagi, H., Yura, T., and Mori, K. (1998) *J. Biol. Chem.* **273,** 33741–33749
28. Yoshida, H., Okada, T., Haze, K., Yanagi, H., Yura, T., Negishi, M., and Mori, K. (2000) *Mol. Cell. Biol.* **20,** 6755–6767
29. Harding, H. P., Zhang, Y., and Ron, D. (1999) *Nature* **397,** 271–274
30. Shi, Y., Vattem, K. M., Sood, R., An, J., Liang, J., Stramm, L., and Wek, R. C. (1998) *Mol. Cell. Biol.* **18,** 7499–7509
31. Harding, H. P., Zhang, Y., Bertolotti, A., Zeng, H., and Ron, D. (2000) *Mol. Cell* **5,** 897–904
32. Delepine, M., Nicolino, M., Barrett, T., Golamaully, M., Lathrop, G. M., and Julier, C. (2000) *Nat. Genet.* **25,** 406–409
33. Harding, H. P., Zeng, H., Zhang, Y., Jungries, R., Chung, P., Plesken, H., Sabatini, D. D., and Ron, D. (2001) *Mol. Cell* **7,** 1153–1163
34. Zhang, P., McGrath, B., Li, S., Frank, A., Zambito, F., Reinert, J., Gannon, M., Ma, K., McNaughton, K., and Cavener, D. R. (2002) *Mol. Cell. Biol.* **22,** 3864–3874
35. Takeda, K., Inoue, H., Tanizawa, Y., Matsuzaki, Y., Oba, J., Watanabe, Y., Shinoda, K., and Oka, Y. (2001) *Hum. Mol. Genet.* **10,** 477–484
36. Hofmann, S., Philbrook, C., Gerbitz, K. D., and Bauer, M. F. (2003) *Hum. Mol. Genet.* **12,** 2003–2012
37. Patil, C., and Walter, P. (2001) *Curr. Opin. Cell Biol.* **13,** 349–355
38. Ishihara, H., Takeda, S., Tamura, A., Takahashi, R., Yamaguchi, S., Takei, D., Yamada, T., Inoue, H., Soga, H., Katagiri, H., Tanizawa, Y., and Oka, Y. (2004) *Hum. Mol. Genet.* **13,** 1159–1170
39. Harding, H. P., Novoa, I., Zhang, Y., Zeng, H., Wek, R., Schapira, M., and Ron, D. (2000) *Mol. Cell* **6,** 1099–1108

Diabetologia (2005) 48: 984–992
DOI 10.1007/s00125-005-1735-1

ARTICLE

N. Shojima · T. Ogihara · K. Inukai · M. Fujishiro · H. Sakoda · A. Kushiyama · H. Katagiri · M. Anai · H. Ono · Y. Fukushima · N. Horike · A. Y. I. Viana · Y. Uchijima · H. Kurihara · T. Asano

Serum concentrations of resistin-like molecules β and γ are elevated in high-fat-fed and obese *db/db* mice, with increased production in the intestinal tract and bone marrow

Received: 2 June 2004 / Accepted: 3 December 2004 / Published online: 15 April 2005

Abstract *Aims/hypothesis:* Resistin and the resistin-like molecules (RELMs) comprise a novel class of cysteine-rich proteins. Among the RELMs, RELMβ and RELMγ are produced in non-adipocyte tissues, but the regulation of their expression and their physiological roles are largely unknown. We investigated in mice the tissue distribution and dimer formation of RELMβ and RELMγ and then examined whether their serum concentrations and tissue expression levels are related to insulin resistance. *Methods:* Specific antibodies against RELMβ and RELMγ were generated. Dimer formation was examined using COS cells and the colon. RELMβ and RELMγ tissue localisation and expression levels were analysed by an RNase protection assay, immunoblotting and immunohistochemical study. Serum concentrations in high-fat-fed and *db/db* mice were also measured using the specific antibodies. *Results:* The intestinal tract produces RELMβ and RELMγ, and colonic epithelial cells in particular express both RELMβ and RELMγ. In addition, RELMβ and RELMγ were shown to form a homodimer and a heterodimer with each other, in an overexpression system using cultured cells, and in mouse colon and serum. Serum RELMβ and RELMγ levels in high-fat-fed mice were markedly higher than those in mice fed normal chow. Serum RELMβ and RELMγ concentrations were also clearly higher in *db/db* mice than in lean littermates. Tissue expression levels revealed that elevated serum concentrations of RELMβ and RELMγ are attributable to increased production in the colon and bone marrow. *Conclusions/interpretation:* RELMβ and RELMγ form homo/heterodimers, which are secreted into the circulation. Serum concentrations of RELMβ and RELMγ may be a novel intestinal-tract-mediating regulator of insulin sensitivity, possibly involved in insulin resistance induced by obesity and a high-fat diet.

Keywords Bone marrow · *db/db* mice · Heterodimer · High-fat diet · Homodimer · Insulin resistance · Intestinal · Resistin-like molecule β · Resistin-like molecule γ · Serum concentration

Abbreviations FIZZ: found in inflammatory zone · GST: glutathione S-transferase · PPARγ: peroxisome proliferator-activated receptor γ · RELM: resistin-like molecules · XCP: ten-cysteine protein

N. Shojima · M. Fujishiro · H. Sakoda · A. Kushiyama · Y. Fukushima
Department of Internal Medicine,
Graduate School of Medicine,
University of Tokyo,
Tokyo, Japan

T. Ogihara · H. Katagiri
Division of Advanced Therapeutics for Metabolic Diseases,
Centre for Translational and Advanced Animal Research on Human Diseases, Tohoku University
Graduate School of Medicine,
Sendai, Japan

K. Inukai
The Fourth Department of Internal Medicine,
Saitama Medical School,
Iruma-gun, Saitama, Japan

M. Anai · H. Ono
The Institute for Adult Disease,
Asahi Life Foundation,
Tokyo, Japan

N. Horike · A. Y. I. Viana · Y. Uchijima · H. Kurihara · T. Asano (✉)
Department of Physiological Chemistry and Metabolism,
Graduate School of Medicine, University of Tokyo,
7-3-1 Hongo, Bunkyo-ku,
Tokyo, Japan
e-mail: asano-tky@umin.ac.jp
Tel.: +81-3-38155411
Fax: +81-3-58031874

Introduction

Type 2 diabetes is characterised by insulin resistance of peripheral tissues such as the liver and muscle and adipose tissue [1–4]. Recent studies have indicated that adipose

tissue is, in addition to being a lipid storage site, an endocrine organ producing hormones, cytokines and other substances [5–7]. Recently, resistin was newly identified as an adipocyte-secreted protein [8]. Serum resistin levels are reportedly elevated in genetically obese mice and are down-regulated by administration of thiazolidinediones [9, 10], peroxisome proliferator-activated receptor γ (PPARγ) agonists, although contradictory data also exist [11]. Resistin has been demonstrated to antagonise insulin action in cultured cells such as 3T3-L1 adipocytes, as well as in rodents [8]. Resistin knock-out mice exhibited lower blood glucose with reduced hepatic glucose production [12]. Thus resistin could be one of the important adipokines causing insulin resistance.

The presence of resistin-like molecules (RELMs) indicates that resistin belongs to a novel family of cysteine-rich secreted proteins (RELM/found in inflammatory zone [FIZZ]/ten-cysteine protein [XCP]). RELMα/FIZZ1 [13] and RELMβ/FIZZ2 [14] are homologous with resistin/FIZZ3 and expressed mainly in white adipose tissue and the colon respectively [14, 15]. The administration of RELMβ to rats resulted in acute impairment of hepatic insulin sensitivity and glucose metabolism [16], which suggested RELMβ is a link between the intestine and hepatic insulin action. Finally, *RELMγ/FIZZ4/XCP1*, a fourth member of the RELM/FIZZ/XCP family, was identified as a gene with decreased expression in rat nasal respiratory epithelium exposed to cigarette smoke [17]. RELMγ was expressed in the bone marrow, spleen, pancreas and colon, and was revealed to play a role as a cytokine in haematopoiesis [18, 19].

The consensus structure of the RELMs is composed of two domains; one half is the N-terminal, including an N-terminal signal sequence and a variable middle portion, and the other half is the C-terminal domain, which has a highly conserved C-terminal signature sequence containing a unique spacing of the cysteine residues. The N-terminal domains of RELMα, RELMβ and RELMγ are 15, 35 and 17% identical to resistin, whereas the C-terminal domains are 47, 54 and 52% identical to resistin. The C-terminus of RELMγ is highly homologous (84%) with RELMβ. Recently, the crystal structures of resistin and RELMβ were revealed to have a unique multimeric structure [20]. Each protomer is comprised of a 'head' and 'tail' segment and circulates as an assembly of hexamers and trimers, which reflect activation of resistin.

We previously identified RELMγ cDNA independently by PCR using degenerated oligonucleotide primers, and investigated its tissue distribution. Since we succeeded in preparing highly specific antibodies against RELMβ and RELMγ, we were able to detect the endogenous proteins and measure serum concentrations as well as tissue contents of RELMβ and RELMγ in the mouse. In this study, we show for the first time that RELMβ and RELMγ form not only a homodimer but also a heterodimer with each other in both tissue and serum. Interestingly, we also found that the serum concentrations of RELMβ and RELMγ are significantly elevated in high-fat-diet-induced and obese diabetic mice. These observations are probably attributable to increased production in the colon and bone marrow. Thus, this report is the first to raise the possibility of a novel intestinal-tract-mediating regulatory mechanism of insulin sensitivity, which may be involved in insulin resistance induced by obesity and a high-fat diet.

Materials and methods

cDNA cloning of a novel RELM/FIZZ isoform Two degenerate oligonucleotide primers were synthesised for PCR. These primers were 5′-ATGAAGA/CCTACAA/CC/TT/GTGTTC/TC-3′ and 5′-TTAG/AGA/CCAG/TTT/CGGC GCAGCG-3′, corresponding to amino acid residues 1–8 and 104–111 of RELMα/β, which are highly conserved among RELM/FIZZ isoforms. PCR was performed using mouse embryonic cDNA. A DNA fragment of approximately 330 bp was then separated by electrophoresis, cloned into TA vector pCRII (Invitrogen, San Diego, CA, USA), and sequenced using a DNA sequencer. We obtained two independent sequences: one, F1, turned out to be completely homologous to mouse RELMα/FIZZ1; the other, F2, encoded a protein to mouse RELMγ/FIZZ4. Then, a mouse embryonic cDNA library produced by a standard method (Stratagene, La Jolla, CA, USA) was screened under standard hybridisation conditions using a ^{32}P-labelled F2 cDNA fragment as a probe to obtain a full-length cDNA encoding RELMγ/FIZZ4. Positive clones were excised into pBluescript and sequenced.

RNase protection assay of various tissues Mice were killed by cervical dislocation, and various tissues (cerebrum, cerebellum, brainstem, heart, lung, liver, oesophagus, stomach, jejunum, ileum, colon, kidney, testis, spleen, pancreas, abdominal fat, epididymal fat, muscle, aorta, femoral bone marrow) were removed. Total RNA was isolated with Isogen (Nippon Gene, Japan). [α-^{32}P]UTP-labelled RNA probes were prepared using nucleotides 1–200 of mouse RELMβ, and 83–315 of mouse RELMγ as templates. An RNase protection assay was performed using an RPA III kit (Ambion, Austin, TX, USA) according to the manufacturer's instructions.

Preparation of the antibodies An antibody against the whole mouse resistin molecule was prepared by immunising rabbits with the recombinant mouse resistin protein, obtained as described previously [21]. Sequences corresponding to nucleotides 11–173 of RELMβ/FIZZ2 and 47–227 of RELMγ/FIZZ4 were amplified by PCR and cloned into the pGEX-3T expression vector (Pharmacia, Piscataway, NJ, USA). Glutathione *S*-transferase (GST) fusion proteins (GST-RELMβ and GST-RELMγ) were prepared according to the manufacturer's instructions (Pharmacia). The antisera were raised by immunising rabbits with GST-RELMβ and GST-RELMγ. From these antisera, an antibody against GST protein was removed by filtering through Affigel-10 covalently coupled to GST proteins. Then, specific antibodies against RELMβ and RELMγ were affinity purified with Affigel-10 covalently

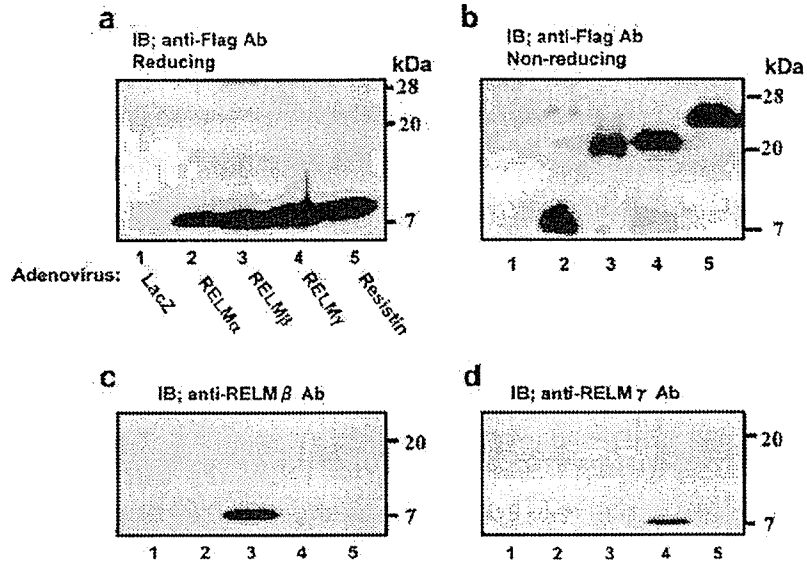

Fig. 1 Immunoblotting of RELMs secreted by COS7 cells. The four cDNAs coding RELMα, RELMβ, RELMγ and resistin, with the Flag tag at their C-termini, were expressed into COS7 cells and the medium from each cell type was subjected to SDS-PAGE under reducing (**a**, **c** and **d**) and non-reducing (**b**) conditions and immunoblotted (IB) with anti-Flag (**a**, **b**), anti-RELMβ (**c**) and anti-RELMγ (**d**) antibody (Ab)

coupled to GST-RELMβ and GST-RELMγ respectively. Antibodies against Flag tag were purchased from Upstate Biotech, Inc. (Lake Placid, NY, USA).

Immunohistochemistry Intestinal tissues removed from the mice were fixed in 10% phosphate-buffered formalin (pH 7.4) and embedded in paraffin. After sectioning, the tissues were dewaxed in ethanol, rehydrated in 10 mmol/l citric acid buffer, and microwaved for 13 min. The tissue sections were blocked with serial incubation in 30% H_2O_2, avidin D-blocking reagent, biotin-blocking reagent and protein-blocking reagent. The sections were then incubated with an affinity-purified polyclonal antibody for murine RELMβ and RELMγ or control serum at a 1:100 dilution overnight at 4°C. After washing with PBS, the slides were incubated with a biotinylated goat anti-rabbit secondary antibody followed by detection of horseradish peroxidase.

Animal studies Nine-week-old male mice (C57BL/6J) were purchased from Jackson Laboratories (Bar Harbor, ME, USA). They were divided into two groups. One group (n=9) was maintained on standard rodent chow, the other (n=9) was fed a high-fat diet (60% fat, 25% carbohydrate and 15% protein). Genetically obese *db/db* mice (n=6) and lean littermates (n=6) were purchased from Jackson Laboratories. They were maintained on standard rodent chow. Tissues from the mice were homogenised in ice-cold lysis buffer. Insoluble materials were removed and the cell lysates were incubated for 2 h at 4°C with the indicated antibody. Blood samples were centrifuged at 3,000 rev/min for 20 min and sera containing equal amounts of protein were used for immunoprecipitation. Immunoblotting against these immunoprecipitates was performed as previously described [21]. Animal care and procedures of the experiments were approved by the Animal Care Committee of the University of Tokyo.

Statistical analysis Data are expressed as means±SE. Comparisons were made using unpaired t-tests. Serum RELM levels were compared with body weight, serum glucose and insulin levels by Pearson's correlation. Values of $p<0.05$ were considered significant.

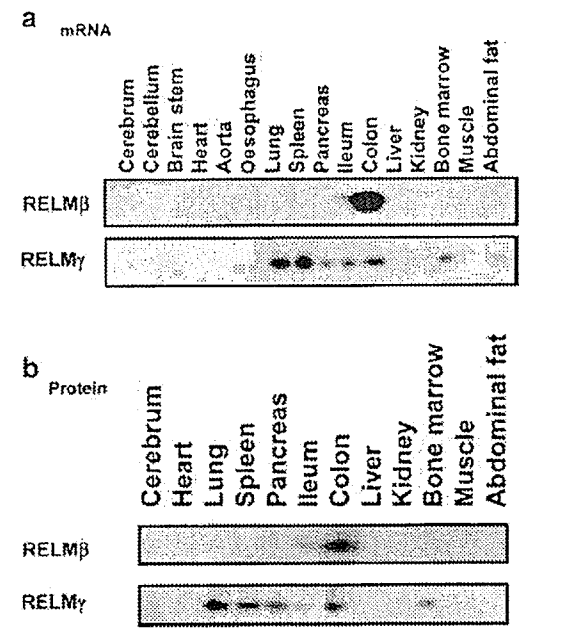

Fig. 2 RELMβ and RELMγ expression in various tissues. **a** 10 μg of RNA from various mouse tissues were prepared and hybridised with [α-^{32}P]UTP-labelled RNA probes for RELMβ or RELMγ. The RNase protection assay was performed using an RPA III kit (Ambion) according to the manufacturer's instructions. **b** Cell lysates from various mouse tissues were prepared and then immunoprecipitated and immunoblotted with anti-RELMβ antibody. Cell lysates from tissues were prepared and then immunoprecipitated and immunoblotted with anti-RELMγ antibody

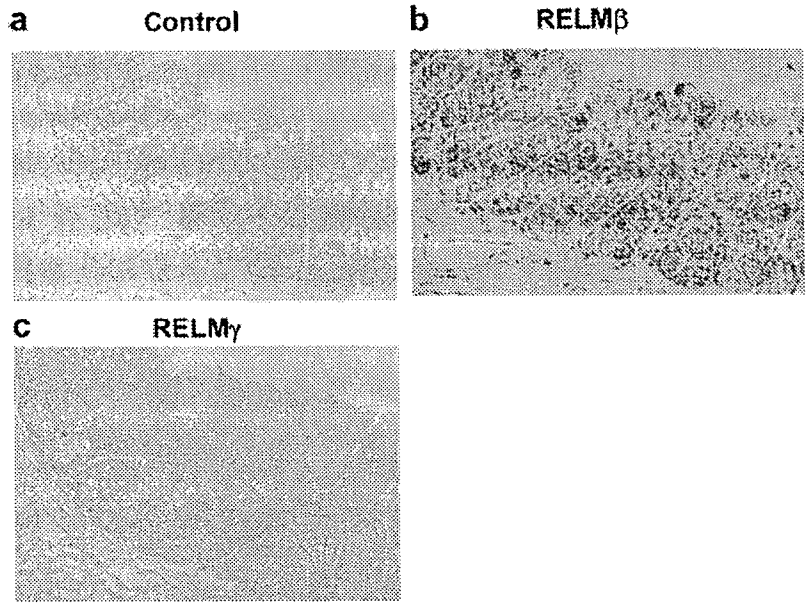

Fig. 3 Immunohistochemical study of RELMβ and RELMγ. Immunohistochemical study of the colon with control antibody (**a**) confirmed the specificities of specific antibodies (×200). The avidin–biotin–peroxidase complex method with antibodies against RELMβ (**b**) and RELMγ (**c**) was used to detect cells expressing these RELMs. RELMβ and RELMγ staining is *brown*, that of the control *blue*

Results

Cloning of RELMγ cDNA To obtain a cDNA fragment corresponding to a novel isoform of RELM/FIZZ, PCR was performed using degenerate oligonucleotides as primers and mouse embryonic cDNA as a substrate. PCR products, with a length of approximately 300–350 bp, were separated, subcloned and sequenced. Isolated PCR products were shown to consist of two different cDNAs. One corresponded to RELMα cDNA [14], the other to RELMγ. The full-length cDNAs encoding resistin, RELMα and RELMβ were prepared by PCRs based on the reported sequences. The full-length cDNA encoding RELMγ was obtained by screening a cDNA library.

Overexpression of RELMs in COS7 cells and preparation of specific antibodies against RELMβ and RELMγ Four cDNAs encoding RELMα, RELMβ, RELMγ and resistin, with the Flag tag at their C-termini, were ligated into adenovirus expression vectors. COS7 cells were infected with these adenoviruses to achieve similar protein expression levels, as assessed by immunoblotting using anti-Flag antibody. The media from cells transfected with these adenoviruses were subjected to SDS-PAGE and immunoblotted with anti-Flag antibody (Fig. 1a). The expression of these proteins was observed as very similar band densities of 7–12 kDa. Thus, it was clear that RELMγ was secreted into the media, like other members of the RELM family, when expressed in COS7 cells.

Next, we investigated the electrophoretic mobilities of these RELMs under non-reducing conditions. As shown in Fig. 1b, RELMβ, RELMγ and resistin migrated with apparent molecular masses twice those of the respective monomers, whereas RELMα behaved as a monomer. Taking previous [22, 23] and current results into account, it was confirmed that resistin, RELMβ and RELMγ form a

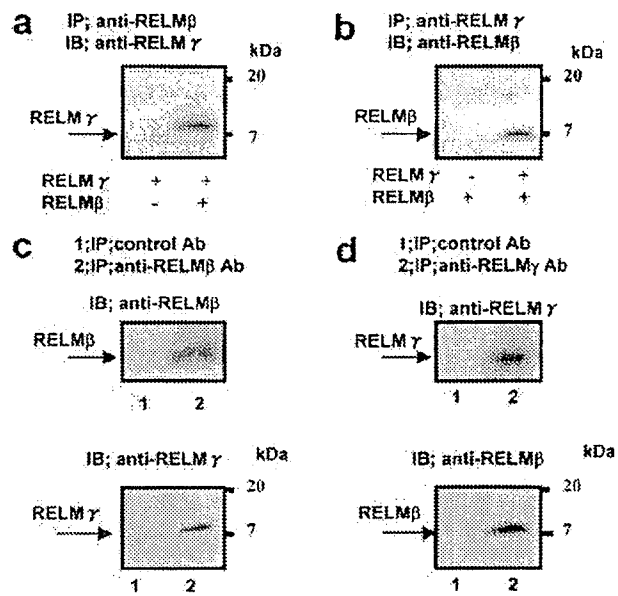

Fig. 4 Heterodimer formations of RELMβ/RELMγ (**a**, **b**) in COS7 cells and endogenous RELMβ/RELMγ in colon (**c**, **d**). **a** Secreted RELMγ, co-expressed with (*right lane*) or without (*left lane*) RELMβ, was immunoprecipitated (*IP*) with anti-RELMβ antibody (*Ab*) and then immunoblotted with anti-RELMγ Ab. **b** RELMβ, co-expressed with (*right lane*) or without (*left lane*) RELMγ was immunoprecipitated with anti-RELMγ Ab and immunoblotted with anti-RELMβ Ab. **c** Colon cell lysates were immunoprecipitated with control IgG (*lane 1*) and anti-RELMβ Ab (*lane 2*) and then immunoblotted with anti-RELMβ Ab (*upper panel*) and anti-RELMγ Ab (*lower panel*). **d** The colon cell lysates were immunoprecipitated with control IgG (*lane 1*) and anti-RELMγ Ab (*lane 2*) and immunoblotted with anti-RELMγ Ab (*upper panel*) or anti-RELMβ Ab (*lower panel*)

Table 1 Serum RELMβ and RELMγ in high-fat-fed mice

	4 weeks		8 weeks		12 weeks	
	Control	High-fat	Control	High-fat	Control	High-fat
RELMβ	1±0.05	1.08±0.06	1±0.05	1.74±0.08[a]	1±0.06	2.16±0.09[a]
RELMγ	1±0.05	1.05±0.05	1±0.06	2.00±0.10[a]	1±0.05	2.70±0.12[a]
RELMβ/γ	1±0.05	0.97±0.06	1±0.05	1.65±0.09[a]	1±0.05	2.54±0.11[a]
Body weight (g)	18.3±1.18	19.3±1.29	26.6±1.32	38.8±2.09[a]	30.1±2.07	44.4±1.95[a]
Glucose (mmol/l)	5.03±0.10	5.11±0.20	5.24±0.16	6.77±0.30	5.13±0.08	7.93±0.27[a]
Insulin (pmol/l)	22.4±1.67	22.7±2.64	26.0±5.00	48.7±2.7[a]	33.1±1.67	62.9±2.45[a]

Male 12-week-old C57BL/6J mice were fed normal chow (n=9) or a high-fat diet (n=9) from 4 to 12 weeks of age. Sera were immunoprecipitated and then immunoblotted with RELMβ and RELMγ antibody. The data are shown as ratios to the control diet values and expressed as means±SE

[a] $p<0.01$ relative to control-diet-fed mice

disulphide-linked dimer, while RELMα exists mainly as a monomer.

Immunoblotting with anti-RELMβ and anti-RELMγ antibodies (Fig. 1c, d) revealed that these antibodies do not recognise other members of the RELM/FIZZ family, suggesting anti-RELMβ and anti-RELMγ antibodies to be highly specific for the corresponding isoforms.

Tissue distribution of RELMβ and RELMγ We next evaluated RELM mRNA expression with an RNase protection assay (Fig. 2a) and protein expression using Western blotting (Fig. 2b) in various mouse tissues. RELMβ mRNA and protein were abundant in the colon, and to a lesser extent in the ileum. On the other hand, RELMγ mRNA was abundant in the colon, ileum, bone marrow, spleen, pancreas and fat, consistent with previous reports [18–20] (Fig. 2a, lower panel). RELMγ protein expression is also detectable in the colon, ileum, bone marrow, spleen and pancreas (Fig. 2b, lower panel). Thus, we found that the colon and ileum express both RELMβ and RELMγ, and the localisations of RELMβ and RELMγ were investigated by immunohistochemical staining of the colon (Fig. 3). It was demonstrated that epithelial cells throughout the crypt and surface of the colon express both RELMβ and RELMγ, while no significant staining was observed with the control antibody. The highest level of RELMβ expression was observed in goblet cells of the colon, consistent with previous reports [15, 24], and RELMγ protein

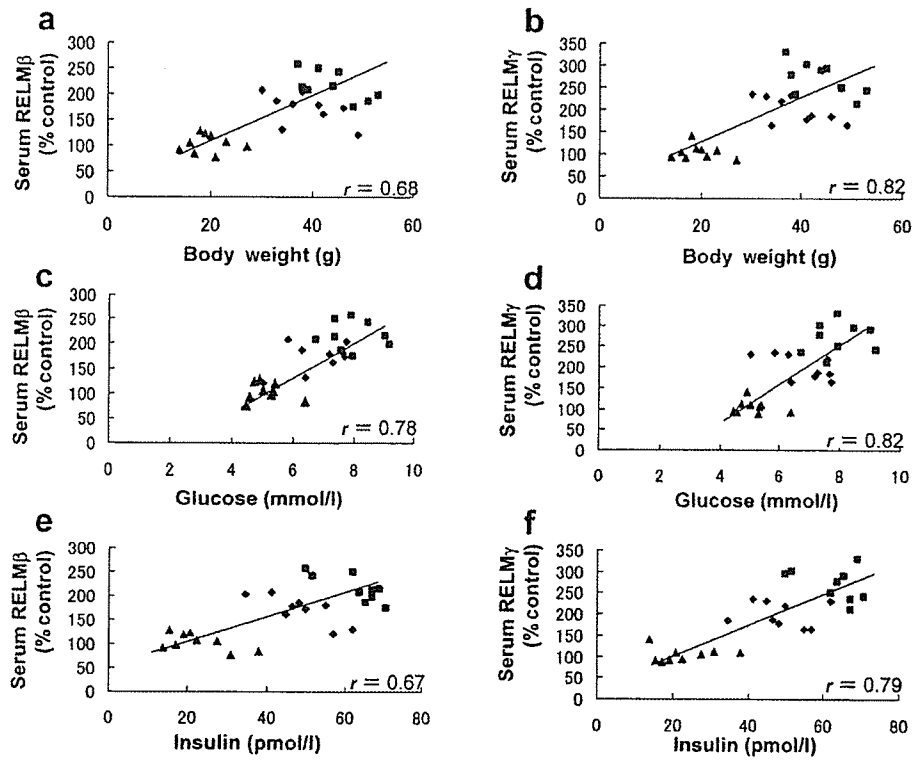

Fig. 5 Relationships between serum RELMβ and RELMγ concentration and body weight, glucose and insulin in high-fat-fed mice. Male 12-week-old C57BL/6J mice were fed normal chow (n=9) or a high-fat diet (n=9) from 4 to 12 weeks of age. RELMβ, RELMγ and various parameters were measured at 4, 8 and 12 weeks of age. The data are plotted as the percentage of the means of RELMβ and RELMγ correlated positively with body weight (**a**, $p<0.0001$; **b**, $p<0.0005$), glucose (**c**, $p<0.0005$; **d**, $p<0.0005$) and insulin (**e**, $p<0.001$; **f**, $p<0.0005$)

Table 2 Expression and regulation of mRNA and protein of RELMβ and RELMγ in high-fat-fed mice

		Colon		Bone marrow		Spleen		Lung		Pancreas	
		Control	High-fat	Control	High-fat	Control	High-fat	Control	High-fat	Control	High-fat
RELMβ	mRNA	1±0.04	1.97±0.04[a]	–	–	–	–	–	–	–	–
	Protein	1±0.03	1.96±0.05[a]	–	–	–	–	–	–	–	–
RELMγ	mRNA	1±0.04	1.84±0.03[a]	1±0.04	1.89±0.05[a]	1±0.04	1.03±0.05	1±0.04	1.05±0.05	1±0.04	0.97±0.05
	Protein	1±0.04	2.04±0.03[a]	1±0.04	1.78±0.05[a]	1±0.03	1.02±0.04	1±0.04	1.03±0.04	1±0.04	0.98±0.05

Male 12-week-old C57BL/6J mice were fed normal chow or a high-fat diet from 4 to 12 weeks of age. RNase protection assay and immunoblotting show RELMβ and RELMγ expression in the colon, bone marrow, spleen, lung and pancreas. The data are shown as ratios to the control diet values and expressed as means±SE

[a] $p<0.01$ relative to control-diet-fed mice

was also shown to be localised in goblet cells. In the bone marrow, about 30% of haematopoietic cells were stained with the anti-RELMγ antibody and these cells were myelocytes and metamyelocytes or neutrophils (data not shown), consistent with previous reports [19, 20].

Heterodimer formation between RELMβ and RELMγ in COS7 cells and tissues Since colonic cells express both RELMβ and RELMγ, we subsequently investigated whether these RELMs form a heterodimer. The RELMβ and RELMγ antibodies were highly specific and did not immunoprecipitate the respective isoforms of RELM (data not shown). As shown in Fig. 4a, b, when RELMβ and RELMγ were co-expressed, RELMγ or RELMβ was detected in the RELMβ or RELMγ immunoprecipitates respectively. These results suggest that RELMβ and RELMγ associate with each other and form a heterodimer.

Subsequently, we investigated whether or not endogenous RELMβ and RELMγ form a heterodimer using the proximal colon. RELMβ was detected in RELMγ immunoprecipitates but not in those of control antibodies (Fig. 4c). RELMγ was also detected in RELMβ immunoprecipitates but not in those of control antibodies (Fig. 4d). These results indicate that the heterodimerisation between RELMβ and RELMγ is physiological.

Increased expression of RELMβ and RELMγ in high-fat-fed mice Male 12-week-old C57BL/6J mice were fed normal chow or a high-fat diet from 4 to 12 weeks of age. A high-fat diet resulted in body weight, serum glucose and insulin increasing time-dependently (30.1±6.21 vs 44.4±5.84 g, 5.13±0.24 vs 7.93±0.81 mmol/l, and 33.1±5.02 vs 62.9±7.35 pmol/l respectively) after 12 weeks of feeding (Table 1). Serum RELMβ and RELMγ levels were increased by 116 and 170% respectively at the end of the 12-week feeding period. We detected the RELMβ/RELMγ heterodimer in serum by immunoblotting of the anti-RELMβ immunoprecipitate with anti-RELMγ antibody, and this heterodimer was also increased.

Serum RELMβ and RELMγ and other parameters were measured at 4, 8 and 12 weeks after initiation of the high-fat diet. Close examination of these three sets of time-dependent data revealed serum RELMβ and RELMγ to correlate positively with body weight (Fig. 5a, $r=0.68$, $p<0.0001$; Fig. 5b, $r=0.82$, $p<0.0005$), serum glucose concentration (Fig. 5c, $r=0.78$, $p<0.0005$; Fig. 5d, $r=0.82$, $p<0.0005$) and serum insulin (Fig. 5e, $r=0.67$, $p<0.001$; Fig. 5f, $r=0.79$, $p<0.0005$).

Subsequently, we investigated the expression levels of RELMβ and RELMγ in tissues at the end of the 12-week feeding period. RELMβ mRNA and protein levels in the distal colon of the high-fat-fed mice were elevated by 97 and 96% respectively (Table 2). Similarly, RELMγ mRNA and protein levels in the distal colon were elevated by 84 and 104% respectively. RELMγ mRNA and protein levels in the bone marrow were also elevated by 89 and 78% respectively. However, no significant alterations were observed in the spleen, lung or pancreas.

Table 3 Serum RELMβ and RELMγ in *db/db* mice

	4 weeks		5 weeks		6 weeks	
	Control	*db/db*	Control	*db/db*	Control	*db/db*
RELMβ	1±0.05	1.34±0.06	1±0.06	1.57±0.09[a]	1±0.07	1.82±0.11[a]
RELMγ	1±0.06	1.68±0.04	1±0.04	1.70±0.08[a]	1±0.04	2.27±0.09[a]
RELMβ/γ	1±0.04	1.48±0.05	1±0.05	1.58±0.08[a]	1±0.05	1.79±0.06[a]
Body weight (g)	19.8±0.90	25.3±0.92	21.0±1.00	27.5±1.13	23.2±0.92	30.1±1.24[a]
Glucose (mmol/l)	4.71±0.12	5.65±0.20	4.94±0.12	5.91±0.22	4.62±0.07	6.13±0.18[a]
Insulin (pmol/l)	21.4±1.64	44.4±2.99	22.0±1.74	48.2±2.63	26.3±1.68	51.9±2.57[a]

Male lean littermates ($n=6$) and *db/db* mice ($n=6$) were fed a standard diet. Sera were immunoprecipitated and then immunoblotted with RELMβ and RELMγ antibody. The data are shown as ratios to the control lean littermate values and expressed as means±SE

[a] $p<0.01$ relative to lean littermates

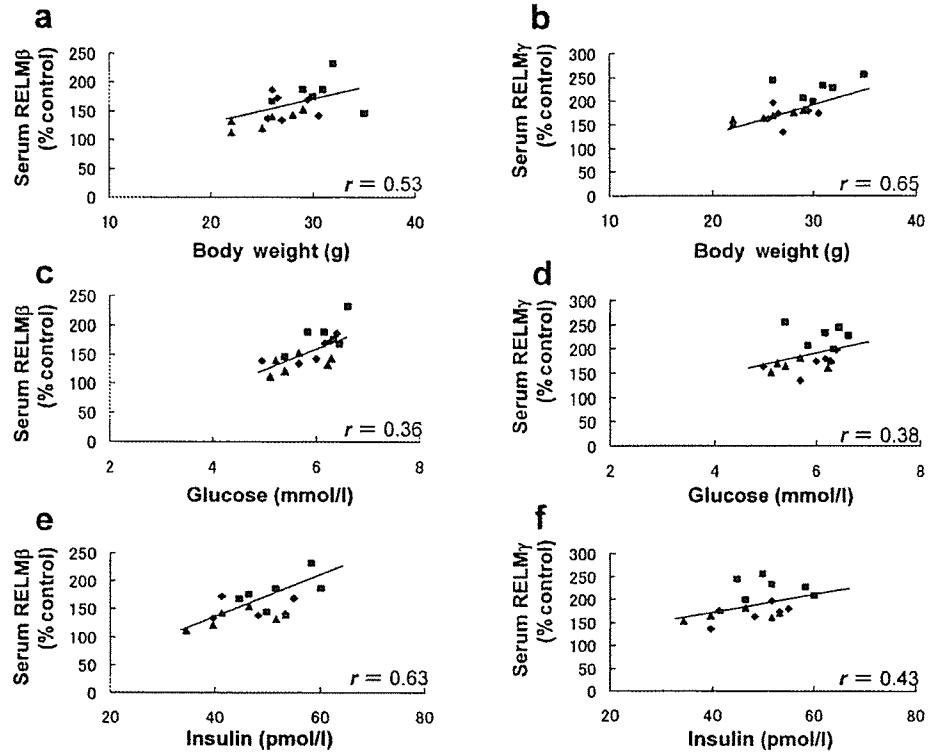

Fig. 6 Relationships between serum RELMβ and RELMγ concentrations and body weight, glucose and insulin in *db/db* mice. Male lean littermates (n=6) and *db/db* mice (n=6) were fed a standard diet. RELMβ, RELMγ and other parameters were measured at 4, 5 and 6 weeks of age. The data are plotted as percentage of the means of control lean littermates. RELMβ and RELMγ correlated positively with body weight (a, $p<0.05$; b, $p<0.01$). Neither RELMβ nor RELMγ showed any correlation with glucose (c, d). RELMβ (e, $p<0.01$), but not RELMγ (f), also positively correlated with insulin

Increased expression of RELMβ and RELMγ in db/db mice Serum RELMβ and RELMγ and other parameters in male *db/db* mice and their littermates were measured at 4, 5 and 6 weeks of age. Male 6-week-old *db/db* mice weighed more (30.1±3.03 vs 23.2±2.26 g), and had higher serum glucose (4.62±0.16 vs 6.13±0.45 mmol/l) and insulin (51.9±6.29 vs 26.3±4.11 pmol/l), than their lean littermates. Serum RELMβ and RELMγ levels of *db/db* mice were higher and were increased by 82 and 127% respectively at the age of 6 weeks, as compared with the controls (Table 3). The RELMβ/RELMγ heterodimer in serum was also increased. Serum RELMβ and RELMγ correlated positively with body weight (Fig. 6a, r=0.53, $p<0.05$; Fig. 6b, r=0.65, $p<0.01$), but not with the serum glucose concentration (Fig. 6c, d). Serum insulin correlated positively with RELMβ (Fig. 6e, r=0.63, $p<0.01$) but not with RELMγ (Fig. 6f).

RELMβ mRNA and protein levels in the distal colons of *db/db* mice at the age of 6 weeks were elevated by 94 and 87% respectively (Table 4). Similarly, RELMγ mRNA and protein levels in the distal colon were elevated by 77 and 98% respectively (Table 4). RELMγ mRNA and protein levels in the bone marrow were elevated by 68 and 53% respectively. There were no significant changes in RELMγ levels in the spleen, lung or pancreas.

Discussion

Resistin and the three RELMs comprise a novel class of cysteine-rich proteins. Resistin is expressed exclusively in adipose tissues and reportedly causes insulin resistance [8]. RELMα was originally identified in broncho–alveolar

Table 4 Expression and regulation of mRNA and protein of RELMβ and RELMγ in *db/db* mice

		Colon		Bone marrow		Spleen		Lung		Pancreas	
		Control	*db/db*	Control	*db/db*	Control	*db/db*	Control	*db/db*	Control	*db/db*
RELMβ	mRNA	1±0.04	1.97±0.07[a]	–	–	–	–	–	–	–	–
	Protein	1±0.05	1.87±0.07[a]	–	–	–	–	–	–	–	–
RELMγ	mRNA	1±0.06	1.77±0.07[a]	1±0.07	1.63±0.07[a]	1±0.04	0.98±0.05	1±0.05	0.96±0.07	1±0.06	1.10±0.07
	Protein	1±0.05	1.98±0.07[a]	1±0.05	1.53±0.07[a]	1±0.06	1.02±0.07	1±0.05	1.05±0.07	1±0.06	1.02±0.07

Male lean littermates and *db/db* mice were fed a standard diet. RNase protection assay and immunoblotting show RELMβ and RELMγ expression in the colon, bone marrow, spleen, lung and pancreas. The data are shown as ratios to the control lean littermate values and expressed as means±SE

[a] $p<0.01$ relative to control-diet-fed mice

lavage fluid in experimentally induced pulmonary inflammation, but is most abundant in adipose tissues [13]. RELMβ is specifically expressed in the intestinal tract, especially abundantly in the colon [14] and has been suggested to be related to bacterial colonisation [24]. Injecting RELMβ reportedly induced insulin resistance in rats [16]. RELMγ is expressed in the colon, bone marrow, spleen and lung [17–19] and reportedly increases the proliferation rate of promyelocytic cells and modulates their differentiation [18]. RELMγ is also expressed in rat nasal respiratory epithelium, and is altered by cigarette smoke [17]. Although the physiological roles of these isoforms are still unclear, a series of previous reports seems to suggest their interaction with inflammatory processes and/or insulin resistance.

In this study we showed that RELMγ overexpressed in and secreted by COS7 cells forms a homodimer. Homodimerisation of RELMβ and resistin, but not RELMα, was previously reported and conserved cysteines (Cys26 of resistin and Cys25 of RELMβ) were considered to be required for disulphide bond formation [23, 24]. In RELMγ, however, the corresponding cysteine is not conserved. Therefore, Cys11 or Cys45 in RELMγ may be regarded as critical for dimer formation. Considering that Cys11 is conserved while Cys45 is missing from RELMα, which is not capable of forming a homodimer, Cys45 in RELMγ is very likely to be involved in dimerisation. Interestingly, we also found that RELMβ and RELMγ secreted by COS7 cells and also endogenously expressed in colonic tissues partially heterodimerised (Fig. 4).

RELMγ reportedly binds α-defensin, a cysteine rich 3–4-kDa antimicrobial peptide stored in the cytoplasimic granules of neutrophils, some macrophages and intestinal Paneth cells [19]. Thus, it is possible that some protein(s), like α-defensin, which bind to RELMγ, also bind to RELMβ and may form polymers with disulphide bonds. In this case, this heteromeric formation may modulate the antimicrobial effects of defensin. In addition, homodimerisation and heterodimerisation of RELMγ would affect binding to other molecules such as their receptor(s) and their resultant functions. Thus, whether or not RELMγ heterodimers and homodimers have different roles in insulin resistance and/or inflammatory processes is important. Further analysis, considering the crystal structure data of resistin and RELMβ, is necessary to clarify the mechanism of homo/heterodimer formation of resistin family proteins [20].

This is the first study to investigate the serum concentrations and tissue contents of RELMβ and RELMγ in insulin-resistant animals, while resistin expression has been analysed in several models of obesity and diabetes [8, 11, 25–30]. In high-fat-fed mice and *db/db* mice, serum levels of RELMβ and RELMγ were apparently increased. Taking into consideration that RELMβ causes insulin resistance by impairing hepatic glucose production [16], it is reasonable to consider the increased serum concentrations of RELMβ and RELMγ to be among the molecular mechanisms underlying the insulin resistance in these diabetic mice. Furthermore, we demonstrated that elevated serum concentrations of RELMβ and RELMγ are attributable to increased production in the colon (both RELMβ and RELMγ) and bone marrow (only RELMγ). Since the heterodimer consisting of serum RELMβ and RELMγ was also increased, a considerable portion of the RELMβ and RELMγ in serum appears to be derived from the colon and ileum.

We observed that the PPARγ agonist rosiglitazone had no effect on expression levels ($10\ mg\ kg^{-1}\ day^{-1}$ for 2 weeks, orally; data not shown). We can suggest two possible mechanisms of RELMβ and RELMγ upregulation in the insulin-resistant diabetic mouse. One involves the expression of these isoforms being regulated by exposure of intestinal and bone marrow cells to nutrients and/or factors such as glucose, lipid, insulin or certain cytokines or hormones. The other involves signals related to inflammation triggering increased RELMβ and RELMγ expression. Since inflammation has mechanistic significance in obesity and insulin resistance [8, 31–34] and some resistin family proteins have been implicated in the inflammatory response [13, 17], increased expression of RELMβ and RELMγ may be involved in the mechanisms connecting inflammation and insulin resistance, which are associated with obesity and/or diabetes. In this regard, a transcriptional factor may be involved in the inflammation-induced increased expression of RELMβ and RELMγ. Indeed, the promoter region of RELMβ contains a binding sequence of nuclear factor κB and signal transducer and activator of transcription 6 [24] and *RELMγ* is reportedly a target gene of CCAAT/enhancer binding protein ε mediating the role of promyelocytic cell development [19]. Our other interesting finding was that the expression of RELMγ was unchanged in the spleen, lung and pancreas in the insulin-resistant as compared with the control mice. A similar observation was that RELMα expression in adipose tissue responds to food deprivation, except in the lung [16]. Thus, it seems that organs specifically responding to nutritional or inflammatory conditions have a system which allows expression of RELMα and RELMγ to be regulated, although the underlying molecular mechanism is unclear.

In summary, adipose tissue and the intestinal tract are major tissues which produce RELM family proteins (resistin and RELMα from adipose tissue, and RELMβ and RELMγ from the intestinal tract). The production of RELMβ and RELMγ in the intestinal tract was clearly demonstrated to be increased in diet-induced and genetically obese mice, with elevated serum concentrations suggesting a hormonal link between the intestinal tract and insulin sensitivity. Furthermore, this link may respond to the total calorie and/or nutrient content of the food ingested. Future studies will examine whether the serum concentrations of RELMβ and RELMγ are also increased in obese or insulin-resistant diabetic human subjects. If so, the measurement of serum RELMβ and RELMγ concentrations may be diagnostically useful. We can also suggest the possibility that RELMβ and RELMγ are potential molecular targets for future antidiabetic drugs, and additional studies are needed to investigate these possibilities.

Acknowledgements We are grateful to Ms Masako Fujita, Ms Kazuyo Shirai and Ms Manami Ikematsu for helping with our experiments in this study.

References

1. Kahn CR (1994) Banting lecture. Insulin action, diabetogenes, and the cause of type II diabetes. Diabetes 43:1066–1084
2. Birnbaum MJ (2001) Turning down insulin signaling. J Clin Invest 108:655–659
3. Saltiel AR, Kahn CR (2002) Insulin signalling and the regulation of glucose and lipid metabolism. Nature 414:799–806
4. Czech MP, Corvera S (1999) Signaling mechanisms that regulate glucose transport. J Biol Chem 274:1865–1868
5. Mora S, Pessin JE (2002) An adipocentric view of signaling and intracellular trafficking. Diabetes Metab Res Rev 18:345–356
6. Kahn BB, Flier JS (2000) Obesity and insulin resistance. J Clin Invest 106:473–481
7. Yamauchi T, Kamon J, Waki H et al (2001) The fat-derived hormone adiponectin reverses insulin resistance associated with both lipoatrophy and obesity. Nat Med 7:941–946
8. Steppan CM, Bailey ST, Brown ER et al (2001) The hormone resistin links obesity to diabetes. Nature 409:307–312
9. Olefsky JM (2000) Treatment of insulin resistance with peroxisome proliferator-activated receptor γ agonists. J Clin Invest 106:467–472
10. Saltiel AR, Olefsky JM (1996) Thiazolidinediones in the treatment of insulin resistance and type II diabetes. Diabetes 45: 1661–1669
11. Way JM, Gorgun CZ, Tong Q et al (2001) Adipose tissue resistin expression is severely suppressed in obesity and stimulated by peroxisome proliferator-activated receptor γ agonists. J Biol Chem 276:25651–25653
12. Banerjee RR, Rangwala SM, Shapiro JS et al (2004) Regulation of fasted blood glucose by resistin. Science 303:1195–1198
13. Holocomb IH, Kadakoff RC, Chan B et al (2000) FIZZ1, a novel cysteine-rich secreted protein associated with pulmonary inflammation, defines a new gene family. EMBO J 19:4046–4055
14. Steppan CM, Brown EJ, Wright CM et al (2001) A family of tissue-specific resistin-like molecules. Proc Natl Acad Sci U S A 98:502–506
15. Rajala MW, Lin Y, Ranalletta M et al (2002) Cell type-specific expression and coregulation of murine resistin and resistin-like molecule α in adipose tissue. Mol Endocrinol 16:1920–1930
16. Rajala MW, Obici S, Sherer PE, Rossetti L (2003) Adipose-derived resistin and gut derived resistin-like molecule-β selectively impair insulin action on glucose production. J Clin Invest 111:225–230
17. Gerstmayer B, Kusters D, Gebel S et al (2003) Identification of RELMγ, a novel resistin-like molecule with a distinct expression pattern. Genomics 81:588–595
18. Schinke T, Haberland M, Jamshidi A et al (2004) Cloning and functional characterization of resistin-like molecule γ. Biochem Biophys Res Commun 314:356–362
19. Chumakov AM, Kubota T, Walter S, Koeffler HP (2004) Identification of murine and human XCP1 genes as C/EBP-ε-dependent members of FIZZ/resistin gene family. Oncogene 23: 3414–3425
20. Patel SD, Rajara MW, Rossetti L et al (2004) Disulfide-dependent multimeric assembly of resistin family hormones. Science 304:1154–1158
21. Ogihara T, Asano T, Ando K et al (2001) Insulin resistance with enhanced insulin signaling in high-salt diet-fed rats. Diabetes 50:573–583
22. Banerjee RR, Lazar MA (2001) Dimerization of resistin and resistin-like molecule is determined by a single cysteine. J Biol Chem 276:25970–25973
23. Chen J, Wang L, Boeg YS, Xia B, Wang J (2002) Differential dimerization and association among resistin family proteins with implications for functional specificity. J Endocrinol 175: 499–504
24. He W, Wang M, Jing H et al (2003) Bacterial colonization leads to the colonic secretion of RELMβ/FIZZ2, a novel goblet cell-specific protein. Gastroenterology 125:1388–1397
25. Le Lay SI, Boucher J, Rey A et al (2001) Decreased resistin expression in mice with different sensitivities to a high-fat diet. Biochem Biophys Res Commun 289:564–567
26. Juan CC, Au LC, Fang VS et al (2001) Suppressed gene expression of adipocyte resistin in an insulin-resistant rat model probably by elevated free fatty acids. Biochem Biophys Res Commun 289:1328–1333
27. Chen L, Nyomba BL (2003) Glucose intolerance and resistin expression in rat offspring exposed to ethanol in utero: modulation by postnatal high-fat diet. Endocrinology 144:500–508
28. Levy JR, Davenport B, Clore JN, Stevens W (2002) Lipid metabolism and resistin gene expression in insulin-resistant Fischer 344 rats. Am J Physiol Endocrinol Metab 282:E626–E633
29. Hirosumi J, Tuncman G, Chang L et al (2002) A central role for JNK in obesity and insulin resistance. Nature 420:333–336
30. Li J, Yu X, Pan W, Unger RH (2002) Gene expression profile of rat adipose tissue at the onset of high-fat-diet obesity. Am J Physiol Endocrinol Metab 282:E1334–E1341
31. Hotamisligil GS, Shargill NS, Spiegelman BM (1993) Adipose expression of tumor necrosis factor alpha: direct role in obesity-linked insulin resistance. Science 259:87–91
32. Miles PD, Romeo OM, Higo K et al (1997) TNFα-induced insulin resistance in vivo and its prevention by troglitazone. Diabetes 46:1678–1683
33. Lehrke M, Lazar MA (2004) Inflamed about obesity. Nat Med 10:126–127
34. Yuan M, Konstantopoulos N, Lee J et al (2001) Reversal of obesity- and diet-induced insulin resistance with salicylates or targeted disruption of Ikkbeta. Science 293:1673–1677

0888-8809/05/$15.00/0
Printed in U.S.A.

Molecular Endocrinology 19(2):379–390

doi: 10.1210/me.2004-0178

Alterations in Mitogen-Activated Protein Kinase Kinase and Extracellular Regulated Kinase Signaling in Theca Cells Contribute to Excessive Androgen Production in Polycystic Ovary Syndrome

Velen L. Nelson-Degrave, Jessica K. Wickenheisser, Karen L. Hendricks, Tomoichiro Asano, Midori Fujishiro, Richard S. Legro, Scot R. Kimball, Jerome F. Strauss, III, and Jan M. McAllister

Departments of Cellular and Molecular Physiology (V.L.N.-D., J.K.W., K.L.H., S.R.K., J.M.M.) and Obstetrics and Gynecology (R.S.L., J.M.M.), Pennsylvania State University College of Medicine, Hershey, Pennsylvania 17033; the Department of Diabetes and Metabolism (T.A., M.F.), Graduate School of Medicine, University of Tokyo, Bunkyo-ku, Tokyo 113-8655, Japan; and the Center for Research on Reproduction and Women's Health (J.F.S.), University of Pennsylvania, Philadelphia, Pennsylvania 19104

We have investigated the involvement of the MAPK signaling pathway in increased androgen biosynthesis and *CYP17* gene expression in women with polycystic ovary syndrome (PCOS). A comparison of MAPK kinase (MEK1/2) and ERK1/2 phosphorylation in propagated normal and PCOS theca cells, revealed that MEK1/2 phosphorylation was decreased more than 70%, and ERK1/2 phosphorylation was reduced 50% in PCOS cells as compared with normal cells. Infection with dominant-negative MEK1 increased CYP17 mRNA and dehydroepiandrosterone (DHEA) abundance, whereas constitutively active MEK1 reduced DHEA production and CYP17 mRNA abundance. Similarly, the MEK inhibitor, PD98059, increased CYP17 mRNA accumulation and *CYP17* promoter activity to levels observed in PCOS cells. Remarkably, in theca cells maintained in the complete absence of insulin, ERK1/2 phosphorylation was decreased in PCOS theca cells as compared with normal theca cells, and CYP17 mRNA and DHEA synthesis were increased in PCOS theca cells. These studies demonstrate that in PCOS cells reduced levels of activated MEK1/2 and ERK1/2 are correlated with increased androgen production, irrespective of the insulin concentration. These findings implicate alterations in the MAPK pathway in the pathogenesis of excessive ovarian androgen production in PCOS. (*Molecular Endocrinology* 19: 379–390, 2005)

POLYCYSTIC OVARY SYNDROME (PCOS) is a disorder that affects approximately 5–10% of reproductive aged women and is characterized by excess androgen production and infertility (1–3). The presence of an elevated level of circulating free testosterone, primarily from increased production of androgens by the ovaries, is the classical endocrine phenotype of women with PCOS (2). There is general agreement that the ovarian theca cell is the primary source of excess androgen biosynthesis in women with PCOS (4–6). Theca cells express a variety of genes encoding components of the steroidogenic pathway that are involved in androgen biosynthesis, in response to the pituitary gonadotropin, LH (7). Of these, the expression of the cytochrome P450 17α-hydroxylase (*CYP17*) gene, which encodes a single cytochrome P450 (P450c17) with both 17α-hydroxylase and C17, 20 lyase activities, is essential for the production of androgens in theca cells (8).

We have previously reported that basal and forskolin-stimulated androgen production is elevated in theca cells isolated from the ovaries of women with PCOS and propagated for successive population doublings (9, 10). We established that increased CYP17 gene transcription, mRNA accumulation, and associated increases in P450 17α-hydroxylase/C17,20 lyase activity are stable characteristics of PCOS theca cells that persist in long-term culture, and thus do not appear to be a consequence of the hormonal milieu that the cells were exposed to *in vivo* (9–12).

To examine the molecular mechanism(s) involved in increased androgen biosynthesis and *CYP17* gene expression in women with PCOS, we have begun to investigate specific components of the MAPK signaling cascade in ovarian theca cells propagated from normal cycling women and women with PCOS. Although regulation of steroidogenic enzyme expression

First Published Online October 28, 2004

Abbreviations: CA-MEK1, Constitutively active MEK1; *CYP17*, gene encoding cytochrome P450c17; DHEA, dehydroepiandrosterone; DN-MEK1, dominant-negative MEK1 molecule; FBS, fetal bovine serum; β-Gal, β-galactosidase; LUC, luciferase; MEK1/2, MAPK kinase; MKP-1, MAPK phosphatase-1; P450c17, P450 17α-hydroxylase/17,20 lyase; PCOS, polycystic ovary syndrome; PD, PD98059; pfu, plaque forming-units; PKB, protein kinase B; TBP, TATA-box binding protein.

***Molecular Endocrinology* is published monthly by The Endocrine Society (http://www.endo-society.org), the foremost professional society serving the endocrine community.**

in theca cells has been largely attributed to LH-dependent increases in adenylate cyclase, more recent studies have provided evidence that alternative signaling pathways, including the MAPK and protein kinase B (AKT) pathways, are associated with LH-induced changes in steroid biosynthesis (13). Similar studies have also demonstrated a role for MAPK signaling in FSH-induced steroid biosynthesis and steroidogenic acute regulatory protein (*STAR*) gene expression in granulosa cells (14–16).

The MAPKs are mediators of signal transduction from the cytosol to the nucleus (17). MAPKs are all proline-directed, serine-threonine kinases that are phosphorylated (*i.e.* activated) on threonine and tyrosine in response to a wide variety of stimuli, including cytokines, growth factors, hormones, cellular stress, and cell adherence (18–20). The signals that link G protein-coupled receptors to the MAPK pathway are complex and may involve the Ras pathway as well as other convergent protein kinase cascades (21). The Ras/MAPK kinase (MEK)/ERK pathway is an important signaling cascade involved in the control of cell proliferation and differentiation. Activation of the ERK1/2 or p42/44 MAPK signaling cascade results from the phosphorylation and activation of MEK1/2 (21). Activation of the ERK pathway stimulates the expression and activity of a number of transcription factors, including members of the Jun, and Fos families, in a cell type-specific manner (17, 20, 22, 23). Pharmacological inhibitors of MEK1 [*i.e.* PD98059 (PD) and U0126], which prevent the activation of ERK1/2 by MEK1/2, have been widely used throughout the literature to examine the role of the ERK1/2 pathway in cellular signaling and differentiation (21, 24, 25).

Although some investigators have suggested that cAMP-stimulated activation of the MEK/ERK signaling cascade augments ovarian steroid biosynthesis (13, 15), others have demonstrated that inhibition of the MEK/ERK signaling cascade is associated with increased steroid biosynthesis (16, 26). In human adrenocortical H295 cells, a reduction in the activation state of the ERK1/2 has also been associated with increased *CYP17* gene expression (27, 28). In the present study, we have begun to evaluate the extent that components of the MEK/ERK signaling cascade may be involved in increased androgen biosynthesis and *CYP17* gene expression in normal and PCOS theca cells. We compared the phosphorylation states of MEK1/2 and ERK1/2 in theca cells propagated from multiple normal and PCOS patients. We used an adenovirus-mediated transfection/infection procedure to over express both the dominant-negative and constitutively active forms of these MEK mutants in theca cells to evaluate the effects of the resultant state of MAPK activation on androgen biosynthesis and CYP17 mRNA abundance. We also examined the effects of the pharmacological MEK1/2 inhibitor, PD, on *CYP17* gene transcription. Because insulin resistance and hyperinsulinemia in PCOS have been hypothesized to contribute to increased androgen production by the ovary, we also examined the extent to which insulin contributes to ERK1/2 phosphorylation in normal and PCOS theca cells.

RESULTS

Phosphorylation of MEK1/2 and ERK1/2 Is Reduced in PCOS Theca Cells

To investigate whether there are differences in MEK/ERK signaling in normal and PCOS theca cells maintained in long-term culture, we compared the phosphorylation states of MEK1/2 and ERK1/2 in fourth-passage theca cells. We examined both the phosphorylated and total forms of MEK1/2 (Fig. 1) and ERK1/2 (Fig. 2) by Western blot analysis in cells that were treated with and without forskolin (20 μM) for 24 h. Our analysis of whole cell lysates harvested from theca cells isolated from five independent normal and PCOS patients, showed that the phosphorylation state of MEK1/ 2 was decreased more than 70% in PCOS theca cells as compared with normal theca cells (Fig. 1). We observed a 50% reduction in the phosphorylation state of ERK1/2 in PCOS cells as compared with normal cells (Fig. 2). ERK1/2 phosphorylation was observed to be decreased in response to forskolin treatment in both normal and PCOS theca cells.

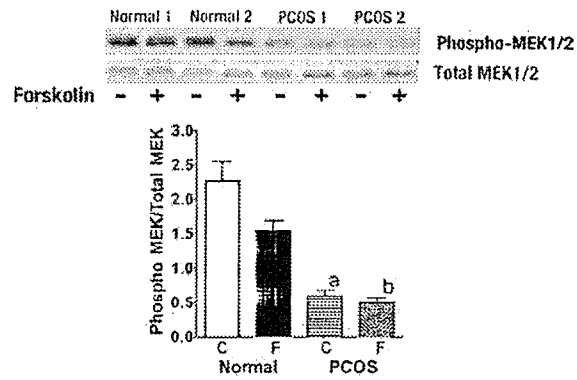

Fig. 1. The Activation State of MEK1/2 Is Decreased in PCOS Theca Cells as Compared with Normal Theca Cells

Fourth-passage theca cells propagated from normal and PCOS patients were grown to confluence and transferred into serum-free medium with vehicle (C) or 20 μM forskolin (F). 24 h thereafter the cells were harvested, and immunnoblot analysis was performed using 35 μg of whole cell extract and antibodies specific for phosphorylated MEK1/2 (Phospho-MEK 1/2) and total MEK. *Upper panel,* Representative immunoblot data of whole cell extracts prepared from theca cells isolated from normal and PCOS patients. *Bottom panel,* Quantitation of the activation state of MEK1/2 in theca cells isolated from five independent normal and PCOS patients is presented. Both basal (a, $P < 0.05$) and forskolin (b, $P < 0.05$)-stimulated MEK1/2 phosphorylation was decreased in PCOS theca cells as compared with normal cells (*, $P < 0.05$).

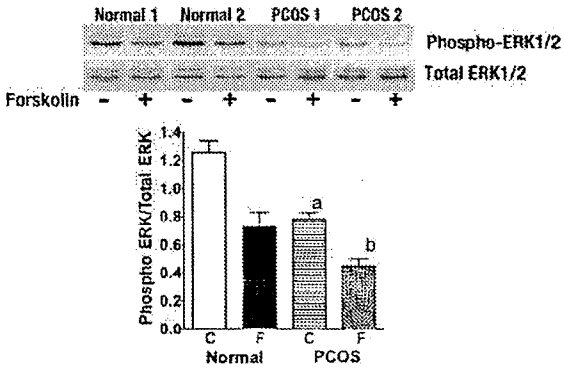

Fig. 2. The Activation State of ERK1/2 Is Decreased in PCOS Theca Cells as Compared with Normal Theca Cells

Fourth-passage theca cells propagated from normal and PCOS patients were grown to confluent and transferred into serum-free medium with vehicle (C) or 20 μM forskolin (F). Twenty-four hours thereafter, the cells were harvested, and immunoblot analysis was performed using 35 μg of whole cell extract and antibodies specific for phosphorylated ERK1/2 (phospho ERK1/2) and total ERK1/2 (ERK1/2). *Upper panel*, Representative immunoblot data of whole cell extracts prepared from theca cells isolated from normal and PCOS patients. *Bottom panel*, Quantitation of the activation state of ERK1/2 in theca cells isolated from five independent normal and PCOS patients is presented. Forskolin treatment resulted in the inhibition of ERK1/2 phosphorylation in both normal and PCOS theca cells. Both basal (a, $P < 0.05$) and forskolin (b, $P < 0.05$)-stimulated ERK1/2 phosphorylation was decreased in PCOS theca cells as compared with normal cells.

MEK and ERK Regulate Thecal Androgen Synthesis

To determine whether the MEK and ERK signaling pathways influence thecal androgen biosynthesis, an adenoviral transfection/infection system was used to examine the effects of a dominant-negative MEK1 molecule (DN-MEK1) (29) on dehydroepiandrosterone (DHEA) production and CYP17 mRNA accumulation in normal theca cells. In these experiments, a half-maximal dose of 7.5 μM forskolin was used to examine possible stimulatory effectors (9). As shown in Fig. 3A, there was a dose-dependent increase in DHEA biosynthesis in response to infection with DN-MEK1 under both basal and forskolin-stimulated conditions, as compared with a control adenovirus expressing β-galactosidase (β-Gal). At a dose of 10–30 plaque forming-units (pfu) of DN-MEK1, which was found to maximally stimulate DHEA biosynthesis 5-fold over forskolin-stimulated conditions, we observed a 50% reduction in ERK1/2 phosphorylation under both basal and forskolin-stimulated conditions (Fig. 3B). We also observed an approximately 2-fold increase in total ERK1/2 after infection with DN-MEK1/2, which effectively reduced the phosphorylation state of ERK1/2. In parallel studies, infection with 10–30 pfu of DN-MEK1 adenovirus significantly increased both basal and forskolin-stimulated CYP17 mRNA abundance (Fig. 3C) and 17α-hydroxylase enzyme activity approximately 2-fold (Fig. 3D).

We used an adenovirus expressing constitutively active MEK1 (CA-MEK1) to examine whether an increase in ERK1/2 activity could reduce DHEA synthesis and CYP17 mRNA accumulation. These studies required using a different adenoviral vector system than that used for DN-MEK1 (Fig. 3) (30) and therefore required using a LacZ control adenovirus. These experiments were performed with a maximal stimulatory dose of 20 μM forskolin so that we could more fully examine the possible inhibitory effects of the MEK1 signaling pathway. As shown in Fig. 4 (*upper panel*), infection of theca cells with CA-MEK1 resulted in an increase in ERK1/2 phosphorylation and a 50% reduction in total ERK1/2. Both basal and forskolin-stimulated DHEA production and CYP17 mRNA abundance were significantly decreased more than 95% and more than 70%, respectively, after infection with CA-MEK1 as compared with control LacZ adenovirus (Fig. 4, *lower* and *middle panels*). These data demonstrate that activation of ERK1/2 directly inhibits thecal CYP17 mRNA accumulation and androgen biosynthesis. Similar results were obtained after infection of PCOS theca cells with CA-MEK1 (data not shown).

To investigate whether inactivation of ERK1/2 signaling directly affects *CYP17* gene expression, we examined the effects of the MEK/ERK pathway-specific pharmacological inhibitor, PD (24) on CYP17 mRNA abundance and promoter function. Evaluation of CYP17 mRNA abundance after PD treatment demonstrated a time-dependent increase in CYP17 mRNA abundance, which was consistent with the results observed after infection with DN-MEK1 (Fig. 3). CYP17 mRNA abundance increased approximately 2-fold in response to 24 h of PD treatment (Fig. 5, *upper panel*). Experiments were performed to assess the effects of PD treatment on DHEA production, however in agreement with the studies of Munir *et al.* (31), we found that PD treatment of theca cells either had no effect or mildly inhibited 17α-hydroxylase enzyme activity as well as DHEA or 17α-hydroxyprogesterone production. From our analysis, it appears that unlike DN-MEK1, PD treatment may nonspecifically inhibit some component of the cytochrome P450 complex.

To examine the effects of PD on the transcriptional regulation of the *CYP17* gene, normal theca cells were transiently transfected with a luciferase (LUC) reporter plasmid containing −750/+44 bp of the 5′ promoter of the human *CYP17* gene. After transfection, the cells were treated with increasing concentrations of PD (0.03–30.0 μM) in the presence and absence of a half-maximal dose of forskolin (7.5 μM). As shown in Fig. 5 (*lower panel*), PD treatment stimulated both basal and forskolin-stimulated *CYP17* promoter activity in a dose-dependent manner with an ED_{50} of approximately 0.5 μM. These experiments were performed in triplicate cultures of

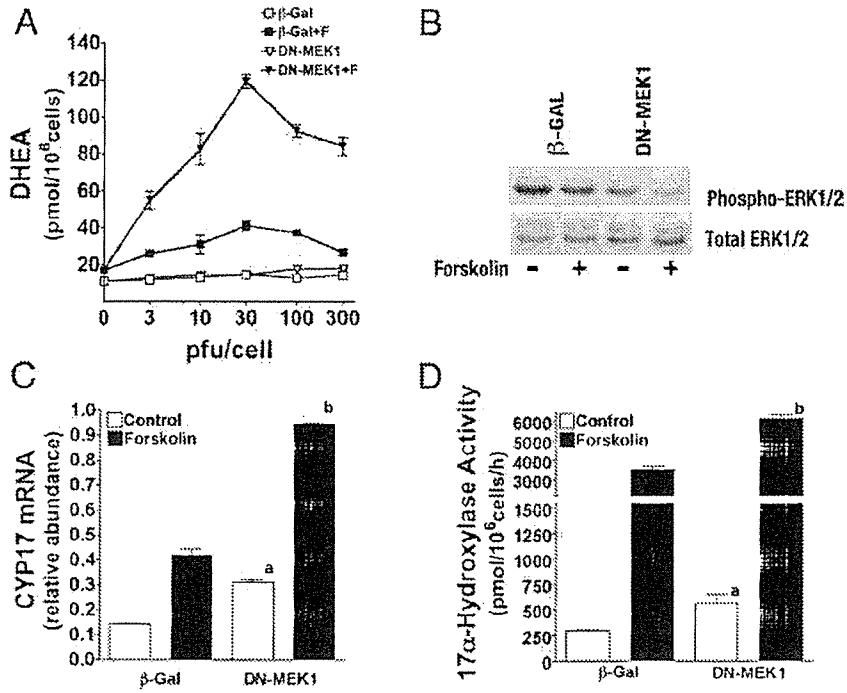

Fig. 3. Inhibition of MEK/ERK Pathway Using a Dominant-Negative MEK1 Adenovirus Augments Thecal Androgen Biosynthesis, 17α-Hydroxylase Enzyme Activity, and CYP17 mRNA Expression

A, To examine the effect of increasing amounts of an adenovirus encoding DN-MEK on thecal androgen biosynthesis, fourth-passage theca cells were grown until subconfluent and were infected with increasing concentrations (3–300 pfu) of either DN-MEK adenovirus or a control β-Gal. Seventy-two hours after treatment with and without forskolin (7.5 μM), the media were collected, and DHEA production was evaluated by RIA. Data were normalized to cell number and results are presented as the mean ± SEM of steroid levels from triplicate theca cell cultures. B, To examine ERK1/2 phosphorylation, fourth-passage theca cells were infected with 10 pfu of either a recombinant adenovirus expressing as a control (β-Gal) or DN-MEK1 and treated with and without 7.5 μM forskolin for 24 h. Thirty-five micrograms of protein isolated from whole cell lysates were subjected to SDS-PAGE and then immunoblotted with antiphospho-ERK (Thr202/Tyr204) antibody. Representative immunoblots from four independent experiments are shown. C, In parallel studies to those performed above, at 24 h CYP17 mRNA abundance was evaluated using quantitative real-time PCR analysis. mRNA accumulation was normalized by TBP mRNA abundance and is depicted graphically as the mean ± SEM. Infection with a DN-MEK1 adenovirus increased both basal (a, $P < 0.05$) and forskolin- (b, $P < 0.05$) stimulated CYP17 mRNA abundance. D, 17α-Hydroxylase enzyme activity was evaluated after infection with DN-MEK or β-Gal adenovirus followed by treatment with and without 7.5 μM forskolin for 72 h, as described in *Materials and Methods*. Infection with a DN-MEK1 adenovirus increased both basal (a, $P < 0.05$) and forskolin- (b, $P < 0.05$) stimulated 17α-hydroxylase enzyme activity.

theca cells isolated from four independent normal patients. Similar results were observed with the MEK1/2 inhibitor U0126 (data not shown) (25).

Inhibition of the ERK1/2 MAPK Pathway with the MEK1 Inhibitor, PD, Differentially Regulates CYP17 Promoter Activity in Normal and PCOS Theca Cells

In view of our data demonstrating that the phosphorylation states of MEK1/2 and ERK1/2 are decreased in PCOS theca cells compared with normal theca cells, we investigated whether pharmacological inhibition of ERK1/2 using PD had similar or differential effects on *CYP17* promoter regulation in normal and PCOS theca cells. In these experiments, normal and PCOS theca cells propagated from five independent normal and PCOS patients were transiently transfected with a pGL3 LUC construct containing −750 to +44 bp of the *CYP17* promoter (−750 CYP17/LUC). After transfection, the cells were treated in the presence or absence of a half-maximal dose of forskolin (7.5 μM), with and without PD (25 μM). In agreement with our preliminary data presented in Fig. 6 (*upper panel*), both basal and forskolin-stimulated CYP17 reporter activity were increased in PCOS theca cells as compared with normal theca cells (11). Treatment of normal cells with PD resulted in an approximately 3-fold increase in basal, and a more than 2-fold increase in forskolin-stimulated reporter activity. In contrast, in PCOS theca cells PD treatment resulted in a less than 1.5-fold increase in both basal and forskolin-stimulated reporter activity. These data demonstrate that *CYP17* gene expression in normal theca cells involves

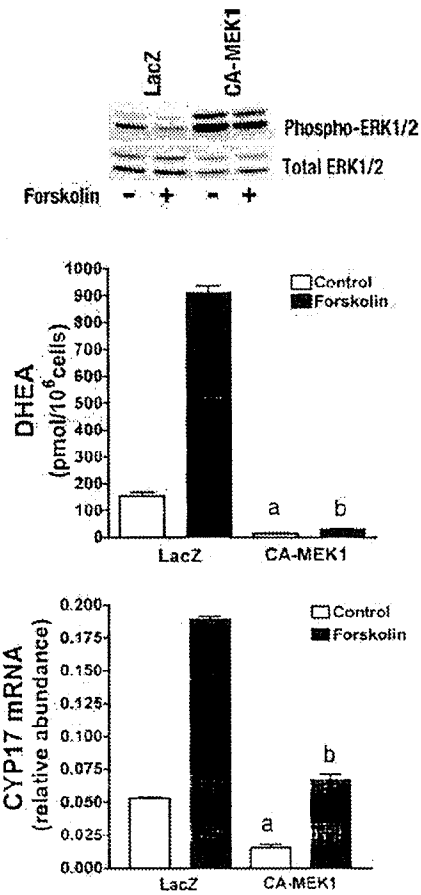

Fig. 4. Constitutively Active MEK Stimulates ERK Phosphorylation and Inhibits DHEA and CYP17 mRNA Abundance

Fourth-passage theca cells were infected with a recombinant adenovirus containing LacZ (control) or CA-MEK1 and treated with and without 20 μM forskolin. *Upper panel*, Twenty-four hours after treatment, the cells were harvested and 35 μg of protein isolated from whole cell lysates were subjected to SDS-PAGE and then immunoblotted with anti-phospho-ERK (Thr202/Tyr204) antibody. Representative immunoblots from four independent experiments are shown. *Middle panel*, Seventy-two hours after treatment, the media were collected and DHEA production was evaluated by RIA. Data were normalized to cell number and are presented as the mean ± SEM from triplicate theca cell cultures that are representative of at least four experiments. Infection with CA-MEK1 inhibited both basal (a, $P < 0.05$) and forskolin-stimulated (b, $P < 0.05$) DHEA production. *Bottom panel*, Fourth-passage theca cells were infected with a recombinant adenovirus containing LacZ or CA-MEK1 and treated with and without 20 μM forskolin. At 24 h, the cells were harvested and CYP17 abundance was evaluated using quantitative real-time PCR analysis. mRNA accumulation was normalized by TBP mRNA abundance and is depicted graphically as the mean ± SEM. Infection with a CA-MEK1 adenovirus inhibited both basal (a, $P < 0.05$) and forskolin (b, $P < 0.05$) stimulated CYP17 abundance.

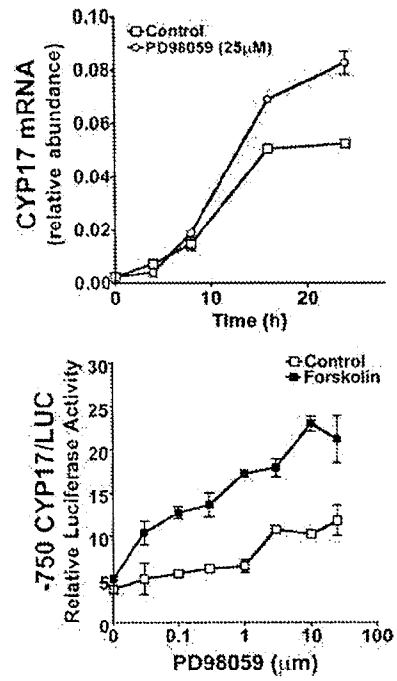

Fig. 5. Inhibition of the ERK1/2 Pathway with the MEK1 Inhibitor PD Augments CYP17 mRNA Accumulation and Promoter Function

Upper panel: Fourth-passage theca cells were treated with and without the MEK1/2 inhibitor PD (25 μM). At 4, 8, 16, 24, and 48 h, the cells were harvested and CYP17 abundance was evaluated using quantitative real-time PCR analysis. mRNA accumulation was normalized by TBP mRNA abundance and is depicted graphically as the mean ± SEM. *Bottom panel:* Fourth-passage theca cells were transiently transfected with a pGL3 LUC construct containing −750 to +44 bp of the *CYP17* promoter (−750 CYP17/LUC). After transfection, the cells were treated with an increasing concentration of PD (0.03–30 μM) with and without a submaximal dose of forskolin (7.5 μM). Seventy-two hours thereafter, the cells were harvested and LUC activity assayed. Data are presented as relative LUC activity that has been corrected for β-Gal activity. Data represent the mean ± SEM of experiments performed with triplicate cultures of theca cells isolated from four normal patients. Inhibition of ERK1/2 signaling using the MEK1 inhibitor PD augmented basal mRNA accumulation and both basal and forskolin-stimulated −750 CYP17/LUC promoter activity in a time and dose-dependent manner ($P < 0.05$).

direct regulation by the ERK pathway. In effect, PD treatment of normal theca cells increased CYP17 promoter activity to the levels observed in PCOS theca cells. In agreement with these findings, in parallel studies PD treatment was observed to inhibit ERK1/2 phosphorylation in normal theca cells to a greater extent than in PCOS theca cells (Fig. 6, *lower panel*).

The Activation State of ERK1/2 Is Decreased, and CYP17 mRNA Abundance and DHEA Biosynthesis Are Increased in PCOS Theca Cells as Compared with Normal Theca Cells Irrespective of the Insulin Concentration

Given the controversial role of insulin in regulating androgen biosynthesis in normal and PCOS theca